A Stochastic Particle-Mesh Scheme for Uncertainty Propagation in Vortical Flows

Olivier P. Le Maître[1] and Omar M. Knio[2]

[1]Laboratoire de Mécanique et d'Energétique d'Evry & LIMSI-CNRS
Université d'Evry Val d'Essonne
40, rue du Pelvoux, CE 1455
91020 Evry cedex, France

[2]Department of Mechanical Engineering
The Johns Hopkins University
Baltimore, MD 21218-2686, USA

Submitted to:
Journal of Computational Physics

Key Words: Particle Method, Uncertainty, Spectral Method, Stochastic Polynomials, Fluid Flow

[1]Corresponding author: Phone (33) 1 69 47 75 31; Fax: (33) 1 69 47 75 99; Email: olm@iup.univ-evry.fr
[2]Email: knio@jhu.edu

Suggested Running Head: Stochastic Polynomial Expansion of Particle Methods

Mailing Address: Olivier P. Le Maître
Universite d'Evry Val d'Essonne - IUP
40, rue du Pelvoux
CE 1455
91 020 Evry cedex, France
Phone: (33) 1 69 47 75 31; Fax: (33) 1 69 47 75 99
Email: olm@iup.univ-evry.fr

Abstract

A new mesh-particle scheme is constructed for uncertainty propagation in vortical flow. The scheme is based on the incorporation of polynomial chaos (PC) expansions into a Lagrangian particle approximation of the Navier-Stokes equations. The main idea of the method is to use a unique set of particles to transport the stochastic modes of the solution. The particles are transported by the mean velocity field, while their stochastic strengths are updated to account for diffusive and convective effects induced by the coupling between stochastic modes. An integral treatment is used for the evaluation of the coupled stochastic terms, following the framework of the particle strength exchange (PSE) methods, which yields a conservative algorithm. It is also shown that it is possible to apply solution algorithms used in deterministic setting, including particle-mesh techniques and particle remeshing. Thus, the method combines the advantages of particles discretizations with the efficiency of PC representations. Validation of the method on uncertain diffusion and convection problems is first performed. An example is then presented of natural convection of a hot patch of fluid in infinite domain, and the computations are used to illustrate the effectiveness of the approach for both large number of particles and high-order PC expansions.

1 Introduction

Simulation of real fluid flows is often challenged by incomplete knowledge of model parameters, including initial conditions, boundary conditions, external forcing, physical properties of the fluid and its constituents. In these situations, one may consider unknown model data as random or uncertain quantities. Thus, it becomes essential to quantify the impact of these uncertainties on the numerical predictions, for instance generating a statistical characterization that can be used to establish confidence measures, estimate limits of predictability, and/or support model-based decision analysis.

Uncertainty propagation and quantification in fluid flows has recently received considerable attention, particularly through the development of efficient spectral techniques based on Polynomial Chaos (PC) expansions. PC based methods were originally developed for engineering problems in solid mechanics [16] and subsequently applied to a large variety of problems, including flow through porous media (*e.g.* [15]), thermal problems (*e.g.* [17, 26, 25, 23, 24]) and reacting systems (*e.g* [10, 28]). PC expansions consist in the representation of the uncertain data as functionals of a finite set of independent random variables with prescribed densities, the uncertainty germ, and in expanding the dependence the model solution using a suitable basis of uncorrelated functionals of the germs. A classical choice for the the basis is a set of polynomials in the germ. If the germ has zero-mean normalized Gaussian components, one obtains the Wiener-Hermite PC basis [32, 3], which is formed of generalized Hermite polynomials. Other density types of the germ components result in various families of orthogonal polynomials or mixtures of orthogonal polynomials [33]. Piecewise polynomials [31] and multi-wavelets [23, 24] were also recently proposed as elements of the basis, as these representations are better suited to account of complex or discontinuous dependencies of the model with regard to the uncertain data. A case-in-point is the occurrence of bifurcation points (or surfaces) within the range of uncertain parameter(s). First applications of PC methods to Navier-Stokes equations appeared in [22, 26, 34]. A review of recent works using PC expansions in Navier-Stokes computations can be found in [18]. To our knowledge, PC expansions have so far been applied to Eulerian fluid flow models, including finite difference, finite element, spectral element, and finite volume approximations. The principal objective of this work is to explore the application of of PC methods in conjunction with Lagrangian particle approximations of the Navier-Stokes equations. As discussed in the extensive exposition of Cottet and Koumoutsakos [8], particles methods have long history [30, 5, 20], are theoretically well-grounded [27, 9] with available convergence results [1, 4, 12, 7]. Their advantages include the flexibility to treat complex and moving boundary problems, the ability to tackle in natural fashion problems in infinite domains, and the ability to deal with problem with low or even vanishing diffusivity. This last feature is particularly attractive as stabilized Eulerian deterministic convection schemes typically rely on upwinding, which are difficult to extend to a stochastic setting, especially when the velocity has large uncertainty. In contrast, Lagrangian particle methods handle

convection in a stable and non-diffusive way. This aspect will consequently be a focus of the present study.

The paper is organized as follows. Section 2 summarizes the formulation of a deterministic particle method, whose extension to the stochastic problems is later carried out in section 3. The extension strategy is based on the use of a unique set of particles to transport all the uncertain modes of the solution. In section 4, a validation of the proposed method is presented by considering two simple problems: the purely diffusive evolution of an uncertain Gaussian vortex, and the non-diffusive convection of a passive scalar by an uncertain velocity field. The validation is performed by comparison with exact solutions. To demonstrate the effectiveness of the proposed technique, the simulation of the natural convection of a localized patch of heated fluid in an infinite domain is considered in section 5. Major conclusions are summarized in section 6, which also provides a brief discussion of further improvement and generalization.

2 Deterministic Particle Method

In this section, we detail the deterministic particle formulation of the problem considered, and discuss acceleration techniques and implementation issues. The deterministic equations of the flow are first presented in section 2.1. In section 2.2, the particle approximation of the deterministic problem is outlined, using integral representations of the diffusion and buoyancy terms. The derivation of these integral kernels is detailed in section 2.3. Diffusion is accounted for using the Particle Strength Exchange (PSE) method of Degond and Mas-Gallic [12], which provides a suitable approach for extending the scheme to the stochastic setting. Buoyancy terms are similarly discretized in a conservative way following the recent work of Eldredge et al. [14]. Section 2.4 discusses the implementation of a particle-mesh method devised to reduce the computational cost of the particle velocity evaluations. Finally, a remeshing procedure for the deterministic problem is briefly discussed in section 2.5.

2.1 Two-dimensional Boussinesq equations

In the Boussinesq limit, the natural convection in an infinite domain of a viscous Newtonian fluid is governed by the incompressible Navier-Stokes equations and the energy conservation equations. For 2D flow, these equations are:

$$\begin{cases} \dfrac{\partial \boldsymbol{u}}{\partial t} + \boldsymbol{u}\cdot\boldsymbol{\nabla}\boldsymbol{u} = -\boldsymbol{\nabla} p + \dfrac{\mathrm{Pr}}{\sqrt{\mathrm{Ra}}}\Delta\boldsymbol{u} + \mathrm{Pr}\theta\boldsymbol{e}_y, \\ \dfrac{\partial \theta}{\partial t} + \boldsymbol{u}\cdot\boldsymbol{\nabla}\theta = \dfrac{1}{\sqrt{\mathrm{Ra}}}\Delta\theta, \\ \boldsymbol{\nabla}\cdot\boldsymbol{u} = 0. \end{cases} \tag{1}$$

where $\boldsymbol{u}(\boldsymbol{x},t)$ is the normalized velocity, $p(\boldsymbol{x},t)$ is the normalized pressure, and $\theta(\boldsymbol{x},t)$ is the normalized temperature. θ is defined according to:

$$\theta = \frac{T - T_{ref}}{\Delta T_{ref}}, \tag{2}$$

where T_{ref} and ΔT_{ref} are the characteristic temperature and temperature difference, respectively. The Boussinesq limit of the Navier-Stokes equations is valid for $\Delta T_{ref}/T_{ref} << 1$, *i.e.* for small characteristic deviations from the reference of the temperature. Variables are normalized with respect to the appropriate combination of reference length L_c, velocity V, time $\tau \equiv L_c/V$, density ρ and pressure $P_c = \rho V^2$. The normalization leads to the usual definitions of Prandtl and Rayleigh numbers, respectively $\mathrm{Pr} = \mu C_p/\kappa$ and $\mathrm{Ra} = \rho g\beta\Delta T_{ref} L_c^3/(\mu\kappa)$, where β is the coefficient of thermal expansion, g is gravitational acceleration, μ and κ are the viscosity and heat conductivity, and C_p the heat capacity of the fluid.

The Boussinesq equations need to be complemented with initial conditions $\boldsymbol{u}(\boldsymbol{x},0)$, $\theta(\boldsymbol{x},0)$, as well as boundary conditions. We shall consider the following

boundary conditions:

$$\boldsymbol{u}(\boldsymbol{x},t)=0,\ \theta(\boldsymbol{x},t)=0 \quad \text{as } |\boldsymbol{x}|\to\infty. \tag{3}$$

Defining the vorticity $\boldsymbol{\omega}=\boldsymbol{\nabla}\wedge\boldsymbol{u}=\omega\boldsymbol{e}_z$, and taking the curl of the momentum equation we obtain:

$$\frac{\partial\omega}{\partial t}+\boldsymbol{\nabla}\cdot(\boldsymbol{u}\omega)=\frac{\mathrm{Pr}}{\sqrt{\mathrm{Ra}}}\Delta\omega+\mathrm{Pr}\frac{\partial\theta}{\partial x}, \tag{4}$$

with initial conditions $\omega(\boldsymbol{x},0)=(\boldsymbol{\nabla}\wedge\boldsymbol{u}(\boldsymbol{x},0))\cdot\boldsymbol{e}_z$ and boundary condition $\omega(\boldsymbol{x},t)=0$ as $|\boldsymbol{x}|\to\infty$. Next, we introduce the stremfunction $\psi(\boldsymbol{x},t)$, defined by:

$$\boldsymbol{u}=\boldsymbol{\nabla}\wedge(\psi\boldsymbol{e}_z), \quad \Delta\psi=-\omega. \tag{5}$$

The normalized governing equations to be solved are then given by:

$$\begin{cases} \dfrac{\partial\omega}{\partial t}+\boldsymbol{\nabla}\cdot(\boldsymbol{u}\omega)=\dfrac{\mathrm{Pr}}{\sqrt{\mathrm{Ra}}}\Delta\omega+\mathrm{Pr}\dfrac{\partial\theta}{\partial x}, \\ \dfrac{\partial\theta}{\partial t}+\boldsymbol{\nabla}\cdot(\boldsymbol{u}\theta)=\dfrac{1}{\sqrt{\mathrm{Ra}}}\Delta\theta, \\ \Delta\psi=-\omega, \\ \boldsymbol{u}=\boldsymbol{\nabla}\wedge(\psi\boldsymbol{e}_z), \\ \omega(\boldsymbol{x},0)=(\boldsymbol{\nabla}\wedge\boldsymbol{u}(\boldsymbol{x},0))\cdot\boldsymbol{e}_z \\ \boldsymbol{u},\omega\to 0 \quad \text{as } |\boldsymbol{x}|\to\infty. \end{cases} \tag{6}$$

2.2 Particle method

The principle of particle methods is to discretize the fluid domain into Lagrangian elements (or particles), which carry vorticity and temperature. The position $\boldsymbol{x}_p$ of a particle obeys:

$$\frac{d\boldsymbol{x}_p}{dt}=\boldsymbol{u}(\boldsymbol{x}_p,t). \tag{7}$$

The velocity and vorticity fields are related through the Biot-Savart integral:

$$\boldsymbol{u}=\frac{-1}{2\pi}\mathcal{K}\star\boldsymbol{\omega}=\frac{-1}{2\pi}\int_{\mathbb{R}^2}\mathcal{K}(\boldsymbol{x},\boldsymbol{y})\wedge\boldsymbol{\omega}d\boldsymbol{y}, \tag{8}$$

with the 2D kernel given by:

$$\mathcal{K}(\boldsymbol{x},\boldsymbol{y})=(\boldsymbol{x}-\boldsymbol{y})/|\boldsymbol{x}-\boldsymbol{y}|^2\ .$$

As discussed further below, the Laplacian and gradient operators can be approximated by integral conservative operators of the form:

$$\begin{aligned} \Delta q &\approx \int_{\mathbb{R}^2} \mathcal{L}(\boldsymbol{x}-\boldsymbol{y})\,[q(\boldsymbol{y})-q(\boldsymbol{x})]\,d\boldsymbol{y}, \\ \frac{\partial q}{\partial x} &\approx \int_{\mathbb{R}^2} \mathcal{G}^x(\boldsymbol{x}-\boldsymbol{y})[q(\boldsymbol{y})+q(\boldsymbol{x})]d\boldsymbol{y}. \end{aligned} \tag{9}$$

With these representations, the transport equations for the vorticity and heat can be recast as:

$$\frac{d\boldsymbol{x}_p}{dt} = \frac{-1}{2\pi}\int_{\mathbb{R}^2} \mathcal{K}(\boldsymbol{x}_p,\boldsymbol{y})\wedge\boldsymbol{\omega}(\boldsymbol{y})d\boldsymbol{y}, \tag{10}$$

$$\begin{aligned} \frac{d\omega}{dt} &= \frac{\mathrm{Pr}}{\sqrt{\mathrm{Ra}}}\int_{\mathbb{R}^2} \mathcal{L}(\boldsymbol{x}_p-\boldsymbol{y})\,[\omega(\boldsymbol{y})-\omega(\boldsymbol{x}_p)]\,d\boldsymbol{y} \\ &+ \mathrm{Pr}\int_{\mathbb{R}^2} \mathcal{G}^x(\boldsymbol{x}_p-\boldsymbol{y})[\theta(\boldsymbol{y})+\theta(\boldsymbol{x}_p)]d\boldsymbol{y}, \end{aligned} \tag{11}$$

$$\frac{d\theta}{dt} = \frac{1}{\sqrt{\mathrm{Ra}}}\int_{\mathbb{R}^2} \mathcal{L}(\boldsymbol{x}_p-\boldsymbol{y})\,[\theta(\boldsymbol{y})-\theta(\boldsymbol{x}_p)]\,d\boldsymbol{y}, \tag{12}$$

where d/dt is the Lagrangian (material) derivative.

The particle discretization relies on a set of Np Lagrangian elements, with associated position $\boldsymbol{X}_i(t)$, circulation $\Gamma_i(t)$ and heat $\Theta_i(t)$. We denote by ϵ the core radius of the particles, and introduce the smoothing function $\zeta_\epsilon(\boldsymbol{x})$ such that $\zeta_\epsilon(\boldsymbol{x})\to\delta(\boldsymbol{x})$ as $\epsilon\to 0$, where δ is the Dirac delta function. The smoothed approximation of the vorticity and temperature fields are

$$\omega(\boldsymbol{x},t)=\sum_{i=1}^{\mathrm{Np}}\Gamma_i(t)\zeta_\epsilon(\boldsymbol{x}-\boldsymbol{X}_i(t)),\quad \theta(\boldsymbol{x},t)=\sum_{i=1}^{\mathrm{Np}}\Theta_i(t)\zeta_\epsilon(\boldsymbol{x}-\boldsymbol{X}_i(t)). \tag{13}$$

Denoting $\mathcal{K}_\epsilon$ the regularized version of $\mathcal{K}$, the evolution equations for the particle positions and strengths are:

$$\frac{d\boldsymbol{X}_i}{dt} = \frac{-1}{2\pi}\sum_{j=1}^{\mathrm{Np}}\Gamma_j\mathcal{K}_\epsilon(\boldsymbol{X}_i,\boldsymbol{X}_j), \tag{14}$$

$$\begin{aligned} \frac{d\Gamma_i}{dt} &= \frac{\mathrm{Pr}}{\sqrt{\mathrm{Ra}}}\sum_{j=1}^{\mathrm{Np}}\mathcal{L}(\boldsymbol{X}_i-\boldsymbol{X}_j)S\,[\Gamma_j-\Gamma_i] \\ &+ \mathrm{Pr}\sum_{j=1}^{\mathrm{Np}}\mathcal{G}^x(\boldsymbol{X}_i-\boldsymbol{X}_j)S[\Theta_j+\Theta_i], \end{aligned} \tag{15}$$

$$\frac{d\Theta_i}{dt} = \frac{1}{\sqrt{\mathrm{Ra}}}\sum_{j=1}^{\mathrm{Np}}\mathcal{L}(\boldsymbol{X}_i-\boldsymbol{X}_j)S\,[\Theta_j-\Theta_i]\,. \tag{16}$$

In the equations above, we used S to denote the volume of the particles, assumed to be the same for all particles. It is seen that the particles move with the local

fluid velocity, while their vorticity and temperature evolve due to diffusion and buoyancy. The initial conditions for the discrete system equations are:

$$\Gamma_i(0) \approx \omega(\boldsymbol{X}_i(0), 0)S, \quad \Theta_i(0) \approx \theta(\boldsymbol{X}_i(0), 0)S. \tag{17}$$

These initial conditions, together with (14-16), constitute a system of ODEs that approximates the continuous system in (6).

2.3 Diffusion and buoyancy terms

As mentioned above, integral representations of the diffusion operator and buoyancy terms are used in the computations. Before outlining these representations, a brief discussion is provided of the rationale behind the present approach. For brevity, the discussion focuses on the diffusion term only. One first notes that the representation announced in (15,16) is not the only means of dealing with diffusion in the context of particle methods. Alternative treatments include random walk and diffusion velocity methods.

In the random walk method [5], diffusion is simulated using random displacement of the particles having a zero mean, and variance proportional to the diffusivity and time step. The strength of the particles, on the other hand, remains unchanged. This approach offers several attractive features, including ease of implementation, the obvious conservative character of the algorithm, and the independence of the random displacements so that particle-particle interactions do not intervene. Unfortunately, extension of the random walk algorithm to stochastic problems tackled using PC representations is generally difficult. An example where severe difficulties arise concerns the case of an uncertain diffusivity, because in this case the variance of the random displacements would be uncertain.

In the diffusion velocity method [13, 29, 2], the diffusion term is recast as a transport term, and diffusion is consequently accounted for by moving the particles using the sum of local convection and diffusion velocities. The particle strength is not affected, and so the method is conservative. Unfortunately, the diffusion velocity method does not appear to be generally well-suited for extension to the uncertain case. As for random walk, uncertainty in the diffusion velocity makes it difficult to devise a particle transport scheme. This difficulty is further compounded by the non-linearities appearing in the definition of the diffusion velocity. Being stochastic, the diffusion velocity must be represented in terms of PC expansions, which adds complexity and may require significant computational overhead.

In order to avoid the difficulties outlined above, the PSE method is adopted for the purpose of modeling diffusion. As further discussed below, PSE amounts to an update of the particle strengths but not of their positions. As further discussed in section 3 below, this feature provides a distinct advantage in a stochastic setting, as it makes possible to define representations involving a single set of particles. The PSE method relies on an integral approximation of the Laplacian, which rely on the definition of a radially-symmetric smoothing

function, ζ_ϵ, defined according to:

$$\zeta_\epsilon(\boldsymbol{x}) \equiv \frac{1}{\epsilon^2}\zeta\left(|\boldsymbol{x}|/\epsilon\right),$$

where ζ is a radial function and ϵ is the core parameter. Following [12], ζ is assumed to satisfy the moment conditions:

$$\int_{\mathbb{R}^2} x^2\zeta(\boldsymbol{x})d\boldsymbol{x} = \int_{\mathbb{R}^2} y^2\zeta(\boldsymbol{x}) = 2,$$
$$\int_{\mathbb{R}^2} x^{\alpha_1}y^{\alpha_2}\zeta(\boldsymbol{x})d\boldsymbol{x} = 0, \quad 1 \leq \alpha_1+\alpha_2 \leq m+1,\ \alpha_1,\alpha_2 \neq 2.$$

Based on these definitions, it can be shown [12] that the Laplacian of a generic scalar field c can be approximated by:

$$\Delta c = \frac{1}{\epsilon^2}\left(\zeta_\epsilon \star c - c\right) + \mathcal{O}(\epsilon^m), \tag{18}$$

where $\star$ denotes the convolution operator.

Applying the approximation above to the vorticity and temperature fields associated with the corresponding smoothed particle representations leads to the following definition of the diffusion kernel,

$$\mathcal{L}(\boldsymbol{x}-\boldsymbol{y}) = \frac{1}{\epsilon^2}\zeta_\epsilon(\boldsymbol{x}-\boldsymbol{y}), \tag{19}$$

which is used in the evolution equations for the particle strengths (15,16). Note that due to the symmetry of the kernel, the diffusion treatment in (15,16) is conservative.

The generalization of the integral approximation of the diffusion operator to derivatives of arbitrary order was recently conducted by Eldredge et al. [14]. They provide the following integral approximation of the derivative operator:

$$D^\beta f \equiv \frac{\partial^{|\beta|}}{\partial x_1^{\beta_1}\ldots\partial x_d^{\beta_d}}f(\boldsymbol{x}) \approx \frac{1}{\epsilon^{|\beta|}}\int[f(\boldsymbol{y})+(-1)^{|\beta|+1}f(\boldsymbol{x})]\zeta_\epsilon^\beta(\boldsymbol{x}-\boldsymbol{y})d\boldsymbol{y}, \tag{20}$$

for positive d-dimensional multi-index β, $|\beta| = \sum_{i=1}^d \beta_i$. They derived constraints on the moments of ζ^β to achieve approximation of arbitrary order, and proposed a set of 2D kernels, for both first derivatives and the Laplacian, with accuracy up to eighth order. In this work, we use the second-order kernel [14]:

$$\zeta(\boldsymbol{x}) = \frac{4}{\pi}\exp[-|\boldsymbol{x}|^2]. \tag{21}$$

Applying the integral approximation of $\partial/\partial x$ to the particle representation leads to:

$$\mathcal{G}^x(\boldsymbol{X}_i,\boldsymbol{X}_j) = \frac{1}{\epsilon}\zeta_\epsilon^x(\boldsymbol{X}_i-\boldsymbol{X}_j), \tag{22}$$

where

$$\zeta^x(\boldsymbol{x}) \equiv -\frac{2x}{\pi}\exp[-|\boldsymbol{x}|^2].$$

The summations in (15,16) suggest that the complexity of the evaluation of the integral diffusion and buoyancy terms are $\mathcal{O}(\mathrm{Np}^2)$. However, the kernels $\zeta_\epsilon^{\Delta,x}$ have fast decay with $\boldsymbol{x}-\boldsymbol{y}$, and so the quadrature can in fact be truncated to particles in a finite neighborhood of the local evaluation point. Specifically, interactions between particles separated by a distance greater than 4ϵ are neglected in the computations. This results in significant reduction of the CPU cost by keeping track of the list of interacting particles, which allows discretizations using a large number of particles.

2.4 Acceleration of velocity computation

The computation of the velocity for all the particles using (14) requires $\mathcal{O}(\mathrm{Np}^2)$ operations. For a large number of particles, the resulting CPU cost is prohibitive. Consequently, fast methods have been proposed to speed-up the evaluation of particles velocity. These include hybrid, or particle-mesh, methods and fast multipole methods.

The multipole methods are based on the idea that one can globally approximate the velocity induced by a cluster of particles, provided that the observation point is located far enough from the cluster. This is usually achieved through multipole expansions, using a hierarchical data structure of the particles distribution. Depending on their construction, the multipole techniques exhibit theoretical computational costs scaling as $\mathcal{O}(\mathrm{Np})$ or $\mathcal{O}(\mathrm{Np}\log\mathrm{Np})$. Unfortunately, application of multipole expansions to stochastic problems appears difficult, since the coefficients of the expansion involve both the particle locations and the (generally random) circulations. Consequently, these methods have not been considered in this work.

The hybrid methods rely on a mesh to compute the velocity field by solving a Poisson's equation for the streamfunction [6]. The procedure involves three steps: the projection step, the resolution of the Poisson's equation and the interpolation step. In the projection step, a mesh covering the particles is constructed and the values of the vorticity field are estimated at the mesh points using a projection operator (see appendix A). The Poisson equation $\Delta\psi = -\omega$ is then solved on the mesh. We rely on Dirichlet boundary conditions that are obtained from the integral representation of the streamfunction:

$$\psi(\boldsymbol{x}) = \int_{\mathbb{R}^2} \mathcal{H}(\boldsymbol{x},\boldsymbol{y})\omega(\boldsymbol{y})d\boldsymbol{y} \approx \sum_{j=1}^{\mathrm{Np}} \Gamma_j \mathcal{H}_\epsilon(\boldsymbol{x},\boldsymbol{X}_j). \tag{23}$$

Once the streamfunction is obtained, numerical differentiation is used to determine the velocity at the mesh points. Second-order centered differences are used for this purpose. The final step consists in interpolating the mesh velocity on the particle positions. Once again, this is achieved by relying on the interpolation formula (see appendix A). For a uniform mesh, with constant

spacing h_g, a fast FFT-based solver is employed to solve the Poisson stream-function equation. The overall CPU cost of the velocity computation thus scales as $\mathcal{O}(\mathrm{Np} + \mathrm{M}\log\mathrm{M})$, where M is the number of mesh points.

2.5 Remeshing

A difficulty inherent to the PSE method is the need to introduce new particles to properly account for the diffusion outside the initial support of ω and θ. Furthermore, as the particles are convected, their spatial distribution can be highly strained and distorted such that they may cease to overlap in some region of the flow. This calls for a remeshing procedure where the fields are periodically rediscretized (see [8] and references therein). This is achieved by considering periodically a new set of particles uniformly distributed on a grid with uniform spacing $\sqrt{S}$ covering the current set of particles. The new particle strengths are computed from the interpolation scheme used for the projection of the vorticity on the velocity mesh. This remeshing introduces a numerical diffusion, inherent to the interpolation procedure, which must be kept as small as possible. In the computations below, this is achieved by remeshing infrequently. Specifically, numerical diffusion due to remeshing was found to be negligibly small, and consequently no special means were needed to reduce it further.

3 Stochastic Spectral Expansions

In this section, we extend the particle method described in the previous section to uncertain flow conditions using PC expansions. The starting point of PC-based methods is the definition of the stochastic basis on which the solution is projected. Essential ingredients for the construction of the stochastic basis and the PC expansion are given in section 3.1. For more details, the reader may refer to [16] for a general exposition of the theory of Wiener-Hermite expansions, to [33] for construction of expansion basis for more general probability measures, and to [23, 24] for wavelet-based decompositions. Once the basis is defined, the corresponding continuous problem is formulated, together with the PC expansion of the solution. It is stressed that this development is generic, *i.e.* it applies to various expansions basis provide the basis is orthogonal. Only the definition of the stochastic multiplication operator would differ. We then proceed in section 3.2 to a straightforward extension of the deterministic particle equations obtained in section 3.1 and show that it results in a cumbersome problem, hardly practical. This first attempt however clearly indicates which characteristics of the particle discretization are desirable to be conserved in the process of PC expansion. With these characteristics in mind, we then propose in section 3.3 an alternative expansion of the particle problem that exhibits the desired properties. Finally, we draw of few remarks concerning the resulting particle formulation of the uncertain flow problem and its connection with the solution method of the deterministic case.

3.1 Stochastic basis and PC expansion

We start with the definition of the expansion basis. Let ξ denote the second-order random vector $\xi = (\xi_1 \dots \xi_{\mathrm{N}})$, with independent components, defined on a probability space $(\Omega, \mathcal{F}, dp)$, with value in $\mathbb{R}^{\mathrm{N}}$, and **prescribed** probability law. Without loss of generality, we shall assume that the ξ_i's are identically distributed, with a density $p(\xi_i)$. Therefore, the density of ξ is

$$p_\xi(\xi) = \prod_{i=1}^{\mathrm{N}} p(\xi_i). \tag{24}$$

Any well-behaved random quantity a, (*e.g.* second-order one), can be expanded in a convergent Fourier-like series of the form

$$a = \sum_{k=0}^{\infty} [a]_k \Psi_k(\xi), \tag{25}$$

where the Ψ_k's are functionals of the random vector ξ and $[a]_k$ are the expansion coefficients, or stochastic modes, of a. For convenience, the functionals Ψ_k are chosen to be orthogonal (uncorrelated), i.e.

$$\langle \Psi_i \Psi_j \rangle = \int_{\mathbb{R}^{\mathrm{N}}} \Psi_i(\xi)\Psi_j(\xi)p(\xi)d\xi = \delta_{ij} \left\langle \Psi_i^2 \right\rangle. \tag{26}$$

Consequently, one has

$$[a]_k = \frac{\langle a\Psi_k \rangle}{\langle \Psi_k^2 \rangle}. \tag{27}$$

Usually, the Ψ_k are polynomials in ξ resulting in the so-called Polynomial Chaos expansion. In fact, when the ξ_i are independent, normalized Gaussian variables, the Ψ_k are multi-dimensional Hermite polynomials. In this work, we shall consider ξ uniformly distributed in $[-1,1]^{\mathrm{N}}$ with a multidimensional Legendre polynomial expansion [33], $p(\xi_i) = 1/2$ for $\xi \in [-1,1]$ and 0 otherwise. Adopting the convention consisting in ordering the polynomial indexes with increasing polynomial order, *i.e.*

$$\Psi_0 = 1, \quad \Psi_{i\in[1,\mathrm{N}]} = \xi_i, \quad \Psi_{\mathrm{N}+1} = \xi_1^2 - 1/2, \quad \ldots, \tag{28}$$

the polynomial expansion of a truncated to order No is

$$a \approx \sum_{k=0}^{\mathrm{P}} [a]_k \Psi_k(\xi), \quad \mathrm{P}+1 = \frac{(\mathrm{N}+\mathrm{No})!}{\mathrm{N}!\mathrm{No}!}. \tag{29}$$

From the indexing convention, we also have the expression of the mean and variance of a:

$$\langle a \rangle = [a]_0, \quad \left\langle (a - \langle a \rangle)^2 \right\rangle \approx \sum_{k=1}^{\mathrm{P}} [a]_k^2 \left\langle \Psi_k^2 \right\rangle. \tag{30}$$

It is emphasized that knowledge of the expansion coefficients $[a]_k$ provides not only the first statistical moments of a, but a complete characterization of a, since one can compute from (29) the probability law of a, the density of ξ being known.

If some data of the problem is uncertain (for instance the initial conditions or some transport properties), the data will be considered as random quantity with an associated probability density functions and corresponding PC expansion. As a result, the flow fields will also be random as the random data appears in the model. Consequently, the flow variables are also functionals of ξ. In general, the system (6) becomes

$$\begin{cases} \dfrac{\partial \omega(\boldsymbol{x},t,\xi)}{\partial t} + \boldsymbol{\nabla} \cdot (\boldsymbol{u}(\boldsymbol{x},t,\xi)\omega(\boldsymbol{x},t,\xi)) = \dfrac{\mathrm{Pr}(\xi)}{\sqrt{\mathrm{Ra}(\xi)}} \Delta\omega(\boldsymbol{x},t,\xi) + \mathrm{Pr}(\xi) \dfrac{\partial \theta(\boldsymbol{x},t,\xi)}{\partial x}, \\ \dfrac{\partial \theta(\xi,t,\xi)}{\partial t} + \boldsymbol{\nabla} \cdot (\boldsymbol{u}(\boldsymbol{x},t,\xi)\theta(\boldsymbol{x},t,\xi)) = \dfrac{1}{\sqrt{\mathrm{Ra}(\xi)}} \Delta\theta(\boldsymbol{x},t,\xi), \\ \Delta\psi(\boldsymbol{x},t,\xi) = -\omega(\xi,t,\xi), \\ \boldsymbol{u}(\xi,t,\xi) = \boldsymbol{\nabla} \wedge (\psi(\boldsymbol{x},t,\xi)\boldsymbol{e}_z), \\ \omega(\boldsymbol{x},0,\xi) = (\boldsymbol{\nabla} \wedge \boldsymbol{u}(\boldsymbol{x},0,\xi)) \cdot \boldsymbol{e}_z, \\ \boldsymbol{u}(\boldsymbol{x},t,\xi), \omega(\boldsymbol{x},t,\xi) \to 0 \quad \text{as } |\boldsymbol{x}| \to \infty. \end{cases} \tag{31}$$

The above system has to be solved in $\mathbb{R}^2 \times [0,T] \times [-1,1]^{\mathrm{N}}$. It is assumed that the probabilistic model of the data are such that the second-order moment of $\mathrm{Ra}^{-1/2}(\xi)$ is finite. It is remarked that (31) involves no differential operator in ξ, a characteristic expressing the independence of deterministic realizations of the flow for different realizations of the data. It is also clear that a numerical approximation of (31) will require an efficient discretization to account for the dependence of the solution on ξ. By expanding the flow variables using the PC basis,

$$[\omega, \theta, \boldsymbol{u}, \psi](\boldsymbol{x}, t, \xi) = \sum_{k=0}^{\infty} [\omega, \theta, \boldsymbol{u}, \psi]_k (\boldsymbol{x}, t) \Psi_k(\xi), \tag{32}$$

it is expected that a low polynomial order will be sufficient to properly represent the solution. In other words, it is expected that the series (32) is quickly convergent such that only a small number P of stochastic modes can be actually retained in the computation. We now focus on the derivation of a particle approximation of the stochastic flow.

3.2 Straightforward particle formulation

A straightforward approach to derive a particle formulation of (31) would consist in considering the particle formulation of the deterministic problem, given by (14-17), and then to allow for a dependence of the variables with ξ. This appears feasible as (31) has no differential operator in the stochastic dimensions. It would result in the following system of stochastic ODEs:

$$\frac{d\boldsymbol{X}_i(t,\xi)}{dt} = \frac{-1}{2\pi} \sum_{j=1}^{\mathrm{Np}} \Gamma_j(t,\xi) \mathcal{K}_\epsilon(\boldsymbol{X}_i(t,\xi), \boldsymbol{X}_j(t,\xi)), \tag{33}$$

$$\begin{aligned} \frac{d\Gamma_i(\xi,t)}{dt} &= \frac{\mathrm{Pr}(\xi)}{\sqrt{\mathrm{Ra}}(\xi)} \sum_{j=1}^{\mathrm{Np}} S\mathcal{L}(\boldsymbol{X}_i(t,\xi) - \boldsymbol{X}_j(t,\xi)) \left[\Gamma_j(t,\xi) - \Gamma_i(t,\xi)\right] \\ &+ \mathrm{Pr}(\xi) \sum_{j=1}^{\mathrm{Np}} S\mathcal{G}^x(\boldsymbol{X}_i(t,\xi) - \boldsymbol{X}_j(t,\xi)) \left[\Theta_j(t,\xi) + \Theta_i(t,\xi)\right], \end{aligned} \tag{34}$$

$$\frac{d\Theta_i(t,\xi)}{dt} = \frac{1}{\sqrt{\mathrm{Ra}}(\xi)} \sum_{j=1}^{\mathrm{Np}} S\mathcal{L}(\boldsymbol{X}_i(t,\xi) - \boldsymbol{X}_j(t,\xi)) \left[\Theta_i(t,\xi) - \Theta_j(t,\xi)\right], \tag{35}$$

$$\Gamma_i(0,\xi) = \omega(\boldsymbol{X}_i(0,\xi),0,\xi)S, \quad \Theta_i(0,\xi) = \theta(\boldsymbol{X}_i(0,\xi),0,\xi)S. \tag{36}$$

A particle representation is thus obtained in which the particles have both random position and strengths. To derive a weak formulation of this problem, the truncated PC expansions of the particles position and strengths,

$$\boldsymbol{X}_i(\xi) = \sum_{k=0}^{\mathrm{P}} [\boldsymbol{X}_i]_k \Psi_k(\xi), \quad \Gamma_i(\xi) = \sum_{k=0}^{\mathrm{P}} [\Gamma_i]_k \Psi_k(\xi), \quad \Theta_i(\xi) \sum_{k=0}^{\mathrm{P}} [\Theta_i]_k \Psi_k(\xi), \tag{37}$$

are introduced into (33-36), which are then projected onto the PC basis. This Galerkin projection yields a system of $\mathrm{P}+1$ coupled problems for the stochastic modes. For instance, the equations for the k-th mode of the particles position are:

$$\left\langle \Psi_k^2 \right\rangle \frac{d[\boldsymbol{X}_i]_k}{dt} = \frac{-1}{2\pi} \sum_{j=1}^{\mathrm{Np}} \left\langle \Psi_k \sum_{l=0}^{\mathrm{P}} [\Gamma_j]_l \Psi_l \mathcal{K}_\epsilon \left(\sum_{m=0}^{\mathrm{P}} [\boldsymbol{X}_i]_m \Psi_m, \sum_{n=0}^{\mathrm{P}} [\boldsymbol{X}_j]_n \Psi_n \right) \right\rangle. \tag{38}$$

We already see from this equation that the approach is cumbersome as the non-linearities of the smoothing kernel $\mathcal{K}_\epsilon$ make it difficult to obtain a true Galerkin representation. A pseudo-spectral technique was proposed in [21] to find the stochastic modes of $\mathcal{K}_\epsilon(\boldsymbol{X}_i(\xi), \boldsymbol{X}_j(\xi))$, but this results in a prohibitively expensive strategy when the number of particles is large. It can be remarked that in the computational strategy for the deterministic problem discussed above, the velocity kernel is never evaluated (if one excepts the boundary conditions for ψ) as the velocity is computed by solving the streamfunction Poisson equation. However, the particle-mesh strategy can not be immediately applied to the present formulation as the stochastic positions of the particles make it difficult to project the vorticity on the mesh; similar difficulties would also arise in the interpolation of the velocity modes at random particle positions. Additional hurdles also include the evaluation of the diffusion and buoyancy terms.

Based on the discussion above, it was concluded that an efficient formulation would involve a set of particles with **deterministic** positions but stochastic strengths. This would avoid the difficulties above, and further enable the use of fast particle-mesh techniques.

3.3 Particle discretization of the stochastic flow

Let us go back to the Eulerian stochastic transport equations for the vorticity and heat. Dropping from the notation the spatial and time dependence of the variables, the conservative form is written as:

$$\begin{cases} \dfrac{\partial \omega(\xi)}{\partial t} + \boldsymbol{\nabla} \cdot (\boldsymbol{u}(\xi)\omega(\xi)) = \dfrac{\mathrm{Pr}(\xi)}{\sqrt{\mathrm{Ra}(\xi)}} \Delta\omega(\xi) + \mathrm{Pr}(\xi) \dfrac{\partial \theta(\xi)}{\partial x}, \\ \dfrac{\partial \theta(\xi)}{\partial t} + \boldsymbol{\nabla} \cdot (\boldsymbol{u}(\xi)\theta(\xi)) = \dfrac{1}{\sqrt{\mathrm{Ra}(\xi)}} \Delta\theta(\xi). \end{cases} \tag{39}$$

For expansions truncated at order No, the weak formulation of the system above is given by the following evolution equations for the stochastic modes:

$$\left\{\begin{array}{l} \dfrac{\partial [\omega]_k}{\partial t} + \displaystyle\sum_{l=0}^{\mathrm{P}}\sum_{m=0}^{\mathrm{P}} C_{klm}\boldsymbol{\nabla}\cdot([\boldsymbol{u}]_l[\omega]_m) = \sum_{l=0}^{\mathrm{P}}\sum_{m=0}^{\mathrm{P}} C_{klm}\left(\left[\dfrac{\mathrm{Pr}}{\sqrt{\mathrm{Ra}}}\right]_l \nabla^2[\omega]_m + [\mathrm{Pr}]_l \dfrac{\partial [\theta]_m}{\partial x}\right), \\ \dfrac{\partial [\theta]_k}{\partial t} + \displaystyle\sum_{l=0}^{\mathrm{P}}\sum_{m=0}^{\mathrm{P}} C_{klm}\boldsymbol{\nabla}\cdot([\boldsymbol{u}]_l[\theta]_m) = \sum_{l=0}^{\mathrm{P}}\sum_{m=0}^{\mathrm{P}} C_{klm}\left[\dfrac{1}{\sqrt{\mathrm{Ra}}}\right]_l \nabla^2[\theta]_m, \end{array}\right. \tag{40}$$

where $C_{klm} \equiv \langle \Psi_k \Psi_l \Psi_m \rangle / \langle \Psi_k^2 \rangle$ is the multiplication tensor. Since by convention $\Psi_0 = 1$, we have $C_{k0k} = 1$ and $C_{k0m} = 0$ for $k \neq m$; Thus the previous equations can be rewritten as:

$$\begin{aligned} \frac{\partial [\omega]_k}{\partial t} + \boldsymbol{\nabla}\cdot([\boldsymbol{u}]_0[\omega]_k) &= -\sum_{l=1}^{\mathrm{P}}\sum_{m=0}^{\mathrm{P}} C_{klm}\boldsymbol{\nabla}\cdot([\boldsymbol{u}]_l[\omega]_m) \\ &+ \sum_{l=0}^{\mathrm{P}}\sum_{m=0}^{\mathrm{P}} C_{klm}\left(\left[\frac{\mathrm{Pr}}{\sqrt{\mathrm{Ra}}}\right]_l \nabla^2[\omega]_m + [\mathrm{Pr}]_l \frac{\partial [\theta]_m}{\partial x}\right) \qquad (41) \\ \frac{\partial [\theta]_k}{\partial t} + \boldsymbol{\nabla}\cdot([\boldsymbol{u}]_0[\omega]_k) &= -\sum_{l=1}^{\mathrm{P}}\sum_{m=0}^{\mathrm{P}} C_{klm}\boldsymbol{\nabla}\cdot([\boldsymbol{u}]_l[\theta]_m) \\ &+ \sum_{l=0}^{\mathrm{P}}\sum_{m=0}^{\mathrm{P}} C_{klm}\left[\frac{1}{\sqrt{\mathrm{Ra}}}\right]_l \nabla^2[\theta]_m. \qquad (42) \end{aligned}$$

Consequently, we can write:

$$\begin{aligned} \frac{D\boldsymbol{x}_p}{Dt} &= [\boldsymbol{u}]_0, \qquad (43) \\ \frac{D[\omega]_k}{Dt} &= -\sum_{l=1}^{\mathrm{P}}\sum_{m=0}^{\mathrm{P}} C_{klm}\int_{\mathbb{R}^2} \mathcal{G}^x(\boldsymbol{x}_p - \boldsymbol{y})\left([u]_l[\omega]_m(\boldsymbol{x}_p) + [u]_l[\omega]_m(\boldsymbol{y})\right) d\boldsymbol{y} \\ &- \sum_{l=1}^{\mathrm{P}}\sum_{m=0}^{\mathrm{P}} C_{klm}\int_{\mathbb{R}^2} \mathcal{G}^y(\boldsymbol{x}_p - \boldsymbol{y})\left([v]_l[\omega]_m(\boldsymbol{x}_p) + [v]_l[\omega]_m(\boldsymbol{y})\right) d\boldsymbol{y} \\ &+ \sum_{l=0}^{\mathrm{P}}\sum_{m=0}^{\mathrm{P}} C_{klm}\left[\frac{\mathrm{Pr}}{\sqrt{\mathrm{Ra}}}\right]_l \int_{\mathbb{R}^2} \mathcal{L}(\boldsymbol{x}_p - \boldsymbol{y})\left([\omega]_m(\boldsymbol{y}) - [\omega]_m(\boldsymbol{x}_p)\right) d\boldsymbol{y} \\ &+ \sum_{l=0}^{\mathrm{P}}\sum_{m=0}^{\mathrm{P}} C_{klm}[\mathrm{Pr}]_l \int_{\mathbb{R}^2} \mathcal{G}^x(\boldsymbol{x}_p - \boldsymbol{y})\left([\theta]_m(\boldsymbol{x}_p) + [\theta]_m(\boldsymbol{y})\right) d\boldsymbol{y}, \qquad (44) \\ \frac{D[\theta]_k}{Dt} &= -\sum_{l=1}^{\mathrm{P}}\sum_{m=0}^{\mathrm{P}} C_{klm}\int_{\mathbb{R}^2} \mathcal{G}^x(\boldsymbol{x}_p - \boldsymbol{y})\left([u]_l[\theta]_m(\boldsymbol{x}_p) + [u]_l[\theta]_m(\boldsymbol{y})\right) d\boldsymbol{y} \\ &- \sum_{l=1}^{\mathrm{P}}\sum_{m=0}^{\mathrm{P}} C_{klm}\int_{\mathbb{R}^2} \mathcal{G}^y(\boldsymbol{x}_p - \boldsymbol{y})\left([v]_l[\theta]_m(\boldsymbol{x}_p) + [v]_l[\theta]_m(\boldsymbol{y})\right) d\boldsymbol{y} \end{aligned}$$

$$+ \quad \sum_{l=0}^{\mathrm{P}} \sum_{m=0}^{\mathrm{P}} C_{klm} \left[\frac{1}{\sqrt{\mathrm{Ra}}}\right]_l \int_{\mathbb{R}^2} \mathcal{L}(\boldsymbol{x}_p - \boldsymbol{y}) \left([\theta]_m(\boldsymbol{y}) - [\theta]_m(\boldsymbol{x}_p)\right) d\boldsymbol{y}. \tag{45}$$

In the previous equation, we have denoted by

$$\frac{Df}{Dt} \equiv \frac{\partial f}{\partial t} + [\boldsymbol{u}]_0 \cdot \boldsymbol{\nabla} f, \tag{46}$$

the particle derivative defined with regard to the mean velocity. The stochastic velocity modes have the integral representation

$$[\boldsymbol{u}]_k(\boldsymbol{x}) = \frac{-1}{2\pi} \int_{\mathbb{R}^2} \mathcal{K}(\boldsymbol{x}, \boldsymbol{y}) [\omega]_k(\boldsymbol{y}) d\boldsymbol{y}. \tag{47}$$

Introducing the smoothed particle approximations of the stochastic vorticity and temperature fields,

$$\omega(\boldsymbol{x}, \xi) = \sum_{i=1}^{\mathrm{Np}} \sum_{k=0}^{\mathrm{P}} [\Gamma_i]_k \Psi_k(\xi) \zeta_\epsilon(\boldsymbol{x}, \boldsymbol{X}_i), \quad \theta(\boldsymbol{x}, \xi) = \sum_{i=1}^{\mathrm{Np}} \sum_{k=0}^{\mathrm{P}} [\Theta_i]_k \Psi_k(\xi) \zeta_\epsilon(\boldsymbol{x}, \boldsymbol{X}_i), \tag{48}$$

and defining the stochastic velocity modes on particle $\boldsymbol{X}_i$ as

$$\boldsymbol{U}_i(\xi) \equiv \sum_{k=0}^{\mathrm{P}} [\boldsymbol{U}_i]_k \Psi_k(\xi), \quad [\boldsymbol{U}_i]_k = \frac{-1}{2\pi} \sum_{j=1}^{\mathrm{Np}} [\Gamma_j]_k \mathcal{K}_\epsilon(\boldsymbol{X}_i, \boldsymbol{X}_j), \tag{49}$$

the particle approximation of (43-45) is given by:

$$\frac{D\boldsymbol{X}_i}{Dt} = [\boldsymbol{U}_i]_0, \tag{50}$$

$$\begin{aligned}
\frac{D[\Gamma_i]_k}{Dt} &= -\sum_{j=1}^{\mathrm{Np}} \sum_{l=1}^{\mathrm{P}} \sum_{m=0}^{\mathrm{P}} C_{klm} S \left\{ \mathcal{G}^x(\boldsymbol{X}_i - \boldsymbol{X}_j) \left([U_i]_l [\Gamma_i]_m + [U_j]_l [\Gamma_j]_m\right) \right. \\
&+ \left. \mathcal{G}^y(\boldsymbol{X}_i - \boldsymbol{X}_j) \left([V_i]_l [\Gamma_i]_m + [V_j]_l [\Gamma_j]_m\right) \right\} \\
&+ \sum_{j=1}^{\mathrm{Np}} \sum_{l=0}^{\mathrm{P}} \sum_{m=0}^{\mathrm{P}} C_{klm} S \left[\frac{\mathrm{Pr}}{\sqrt{\mathrm{Ra}}}\right]_l \mathcal{L}(\boldsymbol{X}_i - \boldsymbol{X}_j) \left([\Gamma_j]_m - [\Gamma_i]_m\right) \\
&+ \sum_{j=1}^{\mathrm{Np}} \sum_{l=0}^{\mathrm{P}} \sum_{m=0}^{\mathrm{P}} C_{klm} S [\mathrm{Pr}]_l \mathcal{G}^x(\boldsymbol{X}_i - \boldsymbol{X}_j) \left([\Theta_i]_m + [\Theta_j]_m\right),
\end{aligned} \tag{51}$$

$$\begin{aligned}
\frac{D[\Theta_i]_k}{Dt} &= -\sum_{j=1}^{\mathrm{Np}} \sum_{l=1}^{\mathrm{P}} \sum_{m=0}^{\mathrm{P}} C_{klm} S \left\{ \mathcal{G}^x(\boldsymbol{X}_i - \boldsymbol{X}_j) \left([U_i]_l [\Theta_i]_m + [U_j]_l [\Theta_j]_m\right) \right. \\
&+ \left. \mathcal{G}^y(\boldsymbol{X}_i - \boldsymbol{X}_j) \left([V_i]_l [\Theta_i]_m + [V_j]_l [\Theta_j]_m\right) \right\} \\
&+ \sum_{j=1}^{\mathrm{Np}} \sum_{l=0}^{\mathrm{P}} \sum_{m=0}^{\mathrm{P}} C_{klm} S \left[\frac{1}{\sqrt{\mathrm{Ra}}}\right]_l \mathcal{L}(\boldsymbol{X}_i - \boldsymbol{X}_j) \left([\Theta_j]_m - [\Theta_i]_m\right),
\end{aligned} \tag{52}$$

for $i = 1, \ldots, \mathrm{Np}$ and $k = 0, \ldots, \mathrm{P}$. The initial conditions for the above system of coupled ODEs are:

$$[\Gamma_i]_k(0) = S\frac{\langle \Psi_k \omega(\boldsymbol{X}_i(0), 0, \xi)\rangle}{\langle \Psi_k^2 \rangle}, \quad [\Theta_i]_k(0) = S\frac{\langle \Psi_k \theta(\boldsymbol{X}_i(0), 0, \xi)\rangle}{\langle \Psi_k^2 \rangle}, \tag{53}$$

for $k = 0, \ldots, \mathrm{P}$ and $i = 1, \ldots, \mathrm{Np}$.

Remarks. As seen from (50), the particles are displaced with the mean velocity field. The stochastic modes of the particle strengths now evolve according to two distinct mechanisms. The first mechanism is the diffusion operator which couples all of the stochastic modes, unless the Rayleigh and Prandtl numbers are both certain. In this case, the stochastic modes independently diffuse with all the same diffusion coefficient $\mathrm{Pr}/\sqrt{\mathrm{Ra}}$ or $1/\sqrt{\mathrm{Ra}}$, for the vorticity and temperature respectively. The second mechanism corresponds to variation in the mode strengths, due to the convection by the stochastic velocity field. If the velocity field is certain, $[\boldsymbol{U}_i]_{k>0} = 0$ for all particles, and only the diffusion and buoyancy terms remain in the right-hand-side of (51-52). Note that $[\boldsymbol{U}_i]_{k>0} = 0$ implies that $[\Gamma_i]_{k>0} = 0$ as well.

An important remark concerns the cost of the evaluation of the stochastic modes of the particles' velocity. Because the particle positions are deterministic, the hybrid mesh-particle method is still practical. The determination of the projection mesh-points and coefficients for each particle is in fact identical to that of the deterministic method. As a consequence, the CPU cost of the computation of velocity modes is roughly $(\mathrm{P} + 1)$ times larger than the cost of the deterministic evaluation for the same number of particles (in fact slightly less as the computation of the projection coefficients is factored on the $\mathrm{P} + 1$ modes). This CPU cost is essentially dominated by the resolution of the Poisson streamfunction equations, which are decoupled. Thus, straightforward parallelization strategies can be envisioned. Similarly, the velocity interpolation at the particle centers involves a unique evaluation of the interpolants which are the same for all the stochastic modes.

Another remark concerns the size of the system of coupled ODEs. For Np particles and $\mathrm{P} + 1$ stochastic modes, we have to advance in time 2Np positions and $2(\mathrm{P} + 1)\mathrm{Np}$ strengths, giving a total of $2(\mathrm{P} + 2)\mathrm{Np}$ variables. The efficiency of the method will thus depend on the ability of the selected basis to represent the uncertainty with a minimal number of stochastic modes. To integrate these ODEs, the deterministic time-stepping scheme can still be used, thus preserving the whole structure of existing deterministic particles code. Only a the evaluation of the right-hand-side of the ODEs is altered. The cost of the ODEs' right-hand-side evaluation is obviously critical for the performance of the method. We have already mentioned that the velocity calculations likely scales with the number of modes for given number of particles, and can be parallelized, at least in the particle-mesh approach. At first glance, it appears that the CPU cost of the evaluation of the right-hand-side of the strength ODEs is $(\mathrm{P} + 1)^3$ times greater than for its deterministic counterpart. This is an overly conservative estimate, because (1) the multiplication tensor is sparse, and (2) since the

particle positions are deterministic many of the integral kernels are identical. In the computations below, we take advantage of this feature by computing and storing the kernels when the near-neighbors lists are constructed. To further improve CPU performance, the stochastic products $\boldsymbol{U}_i\Gamma_i$, $\boldsymbol{U}_i\Theta_i$, $(\mathrm{Pr}/\sqrt{\mathrm{Ra}})\Gamma_i$, $\mathrm{Pr}\Gamma_i$ and $(1/\sqrt{\mathrm{Ra}})\Theta_i$ are first computed, in an efficient vectorized way (with inner loop on particle index) before considering the right-hand-side assembly. Doing so, applications with a large number of particles and high-order expansions are possible even on small platforms, as illustrated in Section 5.

4 Validation

In this section, we present two computational examples of particle simulations with polynomial chaos expansion. Our objective is to validate the proposed extension of the deterministic particle scheme to stochastic situations. To allow for a detailed analysis of the treatment of the stochastic diffusion and convection terms, we consider two examples consisting if the purely diffusive evolution of a circular vortex, and of the purely convective transport of a passive scalar.

4.1 Diffusion of a circular vortex

In this section, we consider the problem of the diffusion of a circular exponential vortex without thermal effect. The governing equation for the vorticity field is

$$\frac{\partial \omega}{\partial t} + \boldsymbol{u} \cdot \boldsymbol{\nabla} \omega = \nu \nabla^2 \omega, \tag{54}$$

with an initial condition of the form

$$\omega(r, t = 0) = \frac{\exp[-r^2/d]}{\pi d}, \quad r = |\boldsymbol{x}|. \tag{55}$$

For this setting, the vortex induces a circular velocity field, with azimuthal component $v(r, t)$ and no radial component. The vortex shape is preserved, but due to diffusion the vortex core spreads with time, and so the velocity field is time dependent. The convective term vanishes, and the diffusion coefficient ν can be lumped with time. Consequently, for uncertain ν, the problem corresponds to uncertainty in the core spreading time scale. We shall consider an uncertain diffusion coefficient of the form:

$$\nu(\xi) = \nu_0 + \nu_1 \xi, \quad \nu_0 = 0.005, \quad \nu_0 = \nu_1/2, \tag{56}$$

where ξ is uniformly distributed on $[-1, 1]$. Thus the diffusion coefficient has a uniform distribution in the range $[0.0025, 0.0075]$. The total circulation of the vortex $\int \omega d\boldsymbol{x} = 1$ is an invariant of the flow, while the total circulations of the stochastic vorticity modes ($k > 0$) are all zero, i.e.

$$\int_{\mathbb{R}^2} [\omega]_k(\boldsymbol{x}, t) d\boldsymbol{x} = 0, \quad \forall t \text{ and } k \geq 1. \tag{57}$$

These identities can also be verified based on the exact expression of the vorticity:

$$\omega_e(r, t, \xi) = \frac{1}{\pi(d + 4\nu(\xi)t)} \exp\left[\frac{-r^2}{d + 4\nu(\xi)t}\right], \tag{58}$$

or the azimuthal velocity:

$$v_e(r, t, \xi) = \frac{1}{2\pi r}\left(1 - \exp\left[\frac{-r^2}{d + 4\nu(\xi)t}\right]\right).$$

For the particle simulation, the complete set of particle equations is solved, including the convection of the particles with the mean velocity field and stochastic coupling terms $\boldsymbol{\nabla}\cdot([\boldsymbol{u}]_l[\omega]_m)$, even though the latter are not expected to contribute because all stochastic modes of the velocity should be orthogonal to the stochastic modes of the vorticity gradient. The problem is solved for an initial condition corresponding to $d = 10\pi\nu_0$. The evolution equations are integrated using a third-order Runge-Kutta scheme with time step $\Delta t = 0.02$. The polynomial order $\mathrm{No} = 5$, so that number of terms in the stochastic polynomial expansion is $\mathrm{P}+1 = 6$. The particle approximation uses a smoothing parameter $\epsilon = 0.05$. The mesh for the Poisson solver has a spacing $h_g = \epsilon$. Remeshing is performed every 10 time steps; the distance between neighboring particles $\sqrt{S} = \epsilon/2$ after remeshing.

In Figure 1, we compare the computed and exact values of the mean and standard deviation of the vorticity as a function of the distance to the vortex center, r, and at different times, $1 \leq t \leq 30$. The computed values reported correspond to the particle approximation on the semi-line $y = 0$, $x \geq 0$, while the exact values are obtained by means of accurate Gauss-Lobatto integrations of the analytic solution (58):

$$\langle \omega_e(r,t,\xi)\rangle = \frac{1}{2}\int_{-1}^{1} \omega_e(r,t,\xi)d\xi, \tag{59}$$

$$\sigma^2(\omega_e(r,t,\xi)) = \frac{1}{2}\int_{-1}^{1} \omega_e^2(r,t,\xi)d\xi - \langle \omega_e(r,t,\xi)\rangle^2 . \tag{60}$$

An excellent agreement is observed for all cases shown in Figure 1. The plots show that as the mean vorticity field spreads, its variance increases (up to $t \approx 10$), followed by a slower decay. The presence of a node point where the standard deviation of $\omega(r)$ exhibits a local minimum is clearly visible. This node slowly moves to larger distance from the vortex center as time progresses.

Figure 2 compares computed and exact radial profiles of the mean and standard deviation of the azimuthal velocity. Again, an excellent agreement between computed and exact solutions is observed. The plots show that at any fixed r, the mean velocity decays monotonically with time. To further interpret the results, we note that the azimuthal velocity $v(r,t)$ is given by the ratio of the circulation the circulation $\gamma(r,t) = 2\pi\int_0^r r'\omega(r',t)dr'$ with $2\pi r$. Regardless of the value of $\nu > 0$, $\gamma(r,t)$ can only decay with time, since vorticity is spreading radially outwards. Thus, for any value of $\nu > 0$, the velocity $v(r,t)$ decays, and so does its mean whatever the density function of ν is. As r increases, however, it takes a longer period of time for diffusion to spread a significant amount of vorticity towards larger radii, and so the mean velocity remains nearly constant for longer period of time as r increases. The interpretation in terms of circulation is also helpful in the examination of the standard deviation of $v(r,t)$. The results show that at given $r > 0$ there is a first period of time where the standard deviation increases, followed by a second stage where it decays. The primary increase of $\sigma(v(r,t))$ results from the uncertainty in ν, that induces an initially growing variability in $\gamma(r,t)$. As time increases, the standard deviation

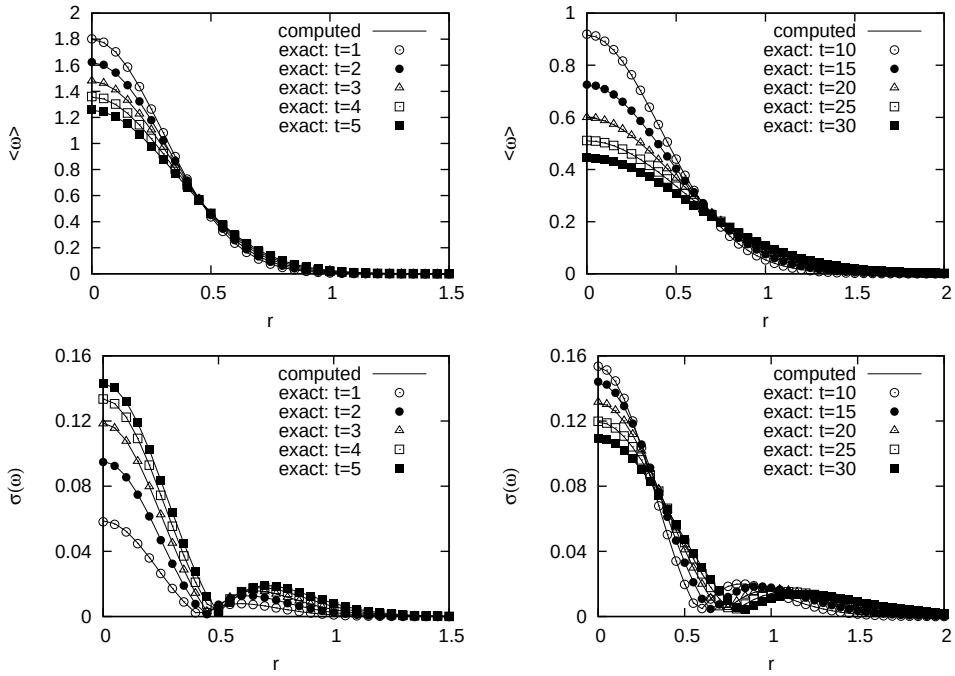

Figure 1: Comparison of numerical (lines) and exact (symbols) values of the mean value of the vorticity $\langle\omega(r,t)\rangle$ (top row) and corresponding standard deviations $\sigma(\omega(r,t))$ (bottom row). Results are presented at time $t = 1$, 2, 3, 4, 5 (left) and $t = 10$, 15, 20, 25 and 30 (right).

in ω decreases as observed earlier; consequently, the standard deviation in γ and in v must decrease as well. As r increases, these trends continue to hold, but are delayed in time and significantly damped.

Figure 3 shows the evolution of the first five stochastic modes $[\omega]_k(r,t)$ for $0 \leq r \leq 2$. Also shown for comparison are profile of the mean mode ω_0. Mode 1 expresses the linear departure from the mean solution as the first Legendre polynomial $\Psi_1 = \xi$. The negative values of $[\omega]_1$ at early times in the neighborhood of the vortex center express the fact that when ν (*i.e.* ξ) increases the diffusion becomes more active and so the vorticity in this region experiences lower values. At larger distance from the vortex center, an increase in the diffusion coefficient yields on the contrary larger vorticity values, and so $[\omega]_1 > 0$ for larger r. It is interesting to note that as time increases, first $[\omega]_1$ quickly increases in magnitude for $r \simeq 0$ before leveling-off for $10 \leq t \leq 30$, and then undergoes a slow decay. It is noted that as time increases, the support of $[\omega]_1$ becomes broader. Higher order stochastic modes also exhibit similar three-stages dynamics (initial increase, leveling-off and slow decay) and broader support as time increases. For higher modes, however, the initial increase is delayed. Furthermore, one observes that $[\omega]_k$ at $r = 0$ is negative for k odd and positive for k even. Finally,

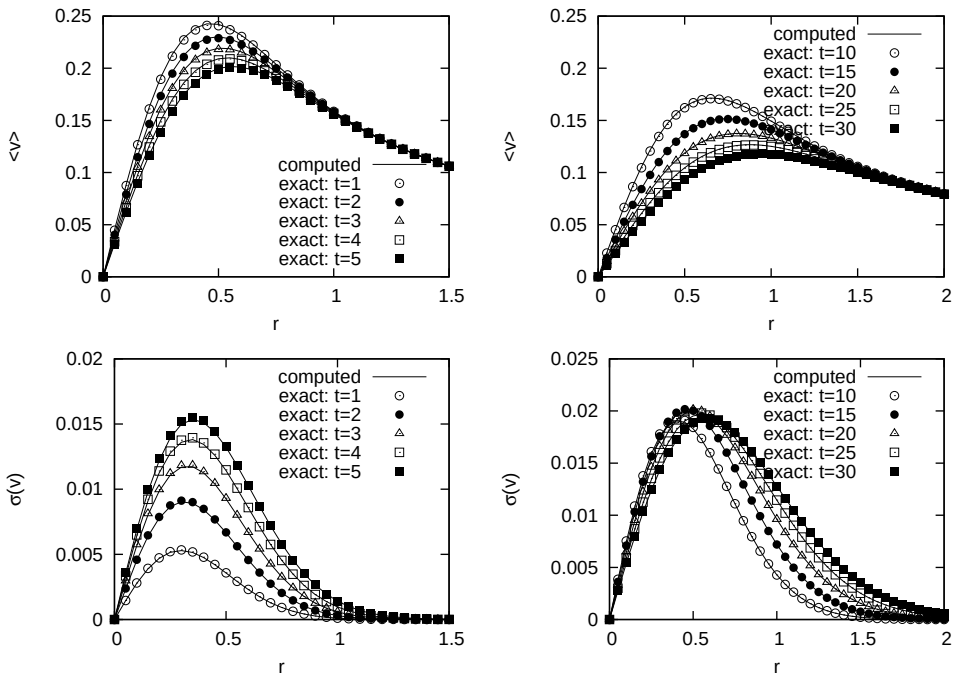

Figure 2: Radial profiles of numerical (lines) and exact (symbols) values of the mean azimuthal velocity $\langle v(r,t)\rangle$ (top row) and its standard deviation $\sigma(v(r,t))$ (bottom row) at corresponding times. Profiles are plotted at time $t = 1$, 2, 3, 4, 5 (left) and $t = 10$, 15, 20, 25 and 30 (right).

one can appreciate the convergence of the stochastic polynomial expansion by noticing the decay in the magnitudes of $[\omega]_k$ as k increases. In fact, a computation with lower order No = 3 revealed no significant differences on the resulting mean and standard deviation fields as reported in Figures 1 and 2.

We finally show in Figure 4 the evolution of the number of particles involved in the simulation. The plot shows a steady increase of the number of particles. As the support of vorticity spreads due to diffusion, more particles are needed for a suitable discretization. In this simulation, the initial number of particles increased from initially Np = 8,192, to Np = 38,720 when the computations were stopped. The CPU time was roughly 3 hours on a desktop PC.

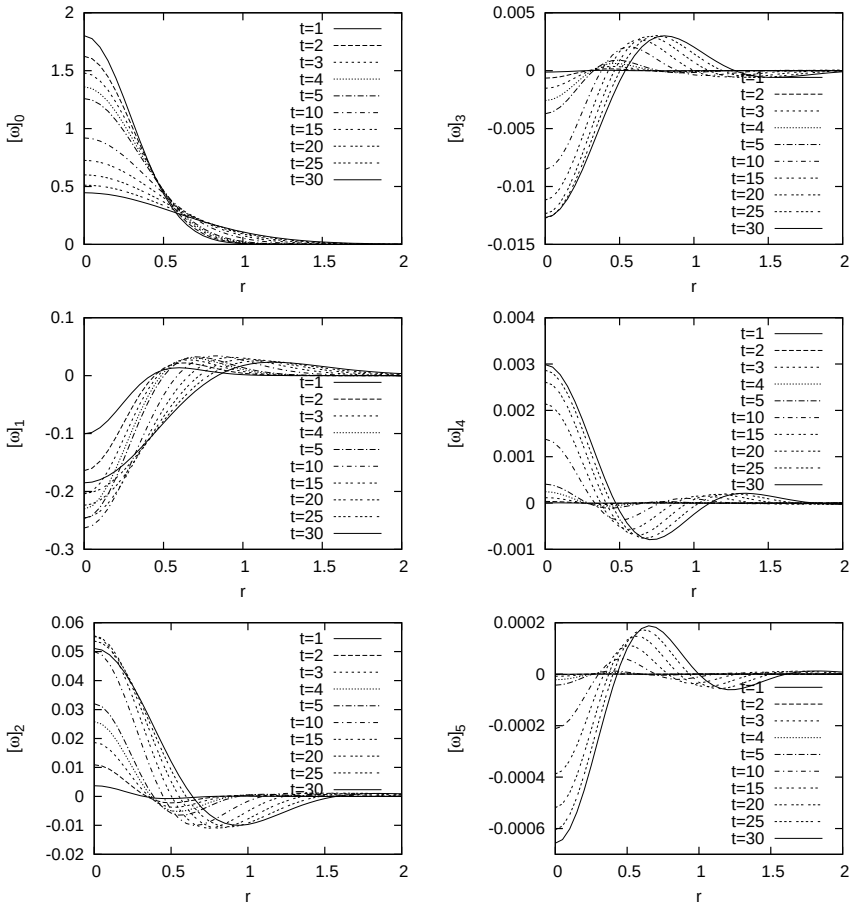

Figure 3: Radial profiles of the vorticity modes $[\omega]_k(r,t)$ plotted at time $t = 1$, 2, 3, 4, 5, 10, 15, 20, 25, 30.

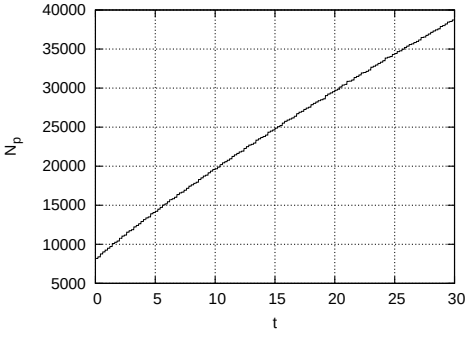

Figure 4: Evolution of the number of particles during the simulation.

4.2 Convection of a passive scalar

In this section, a second test problem is considered which consists of the convection of a passive scalar. The stochastic problem is specified in terms of the transport equation:

$$\frac{\partial c}{\partial t} + \boldsymbol{u} \cdot \boldsymbol{\nabla} c = 0, \tag{61}$$

with given, uncertain, divergence-free velocity field $\boldsymbol{u}$ and the deterministic initial condition:

$$c(\boldsymbol{x}, 0) = \frac{\exp[-r^2/d]}{\pi d}, \quad r = |\boldsymbol{x} - \boldsymbol{c}_0|. \tag{62}$$

We set $\boldsymbol{c}_0 = \boldsymbol{e}_y$, $d = 0.05$ and

$$\boldsymbol{u}(\boldsymbol{x}) = -\boldsymbol{x} \wedge \boldsymbol{e}_z(1 + 0.075\xi). \tag{63}$$

Again, the random variable ξ is assumed to be uniformly distributed over $[-1, 1]$, and so the convective field corresponds to solid rotation about the origin with an uncertain rotational speed of 1 ± 0.075 round(s) per 2π units of time. The center of the concentration field, $\boldsymbol{c}$, evolves according to:

$$\boldsymbol{c}(t, \xi) = \cos\left[\pi/2 + (1 + 0.075\xi)t\right] \boldsymbol{e}_x + \sin\left[\pi/2 + (1 + 0.075\xi)t\right] \boldsymbol{e}_y, \tag{64}$$

and the exact scalar value may be expressed as:

$$c_e(\boldsymbol{x}, t, \xi) = \frac{1}{2d} \exp\left[\frac{-|\boldsymbol{x} - c(t, \xi)|^2}{d}\right]. \tag{65}$$

For the inputs above, at $t = k(2\pi)$ the center of the scalar distribution is uniformly distributed over an arc with length $0.015(2\pi)k \sim 1k$, while the radius of the scalar distribution is estimated as $\sim 2\sqrt{d} \sim 0.5$. These estimates show that the uncertain velocity field induces in just one revolution an uncertainty in the scalar field location which is of the same order as the diameter of the distribution of c. Thus, the present problem constitutes a challenging test, as high-order expansions are needed in order to represent solution at even moderate times. Note that these challenges are inherent to the stochastic nature of the problem, and are not associated with the selected Lagrangian discretization scheme. Specifically, high-order PC expansions would also be needed if an Eulerian discretization scheme is used. Note, however, that in the latter case the numerical solution would face additional difficulties associated with the transport of a non-diffusiving scalar, and that these difficulties would also arise in a deterministic setting. To address these difficulties, Eulerian approaches rely on elaborate discretizations (using for instance flux limiters), but extension of these discretizations to situations involving random velocity fields is not immediate. Particle methods, on the other hand, are well-suited for convection-dominated problems. One of the objectives of the present tests is to verify that this remains the case when the convective field is uncertain.

The problem is first solved for a particle discretization with $\epsilon = 0.025$, a third-order Runge-Kutta scheme with $\Delta t = 2\pi/400$, and large polynomial order No $= 20$. Remeshing is applied every 10 iterations, with spacing $\sqrt{S} = \epsilon/2$. The computed means and standard deviations of the scalar fields after 1 and 2 revolutions, together with the corresponding exact solutions, are plotted in Figure 5. The agreement between particle and solutions is again excellent.

We present in Figure 6 the time-evolution of the spectrum $E_2(k)$, defined according to:

$$E_2(k) = \sum_{i=1}^{\mathrm{Np}} [C_i]_k^2, \tag{66}$$

where C_i is the scalar strength of the i-th particle. E_2 essentially measures the energy in the individual scalar modes. One observes that the energy of mode zero decays, which reflects increasing uncertainty in the location where the scalar is concentrated. The energies of the higher modes $k > 0$ on the contrary steadily increase. It is however observed that the spectra monotonically decrease as k increases, denoting the convergence of the polynomial expansion. However, as time progresses, the decay of the spectrum with k becomes slower, indicating that the number of stochastic modes needed to suitably represent the solution increases with time.

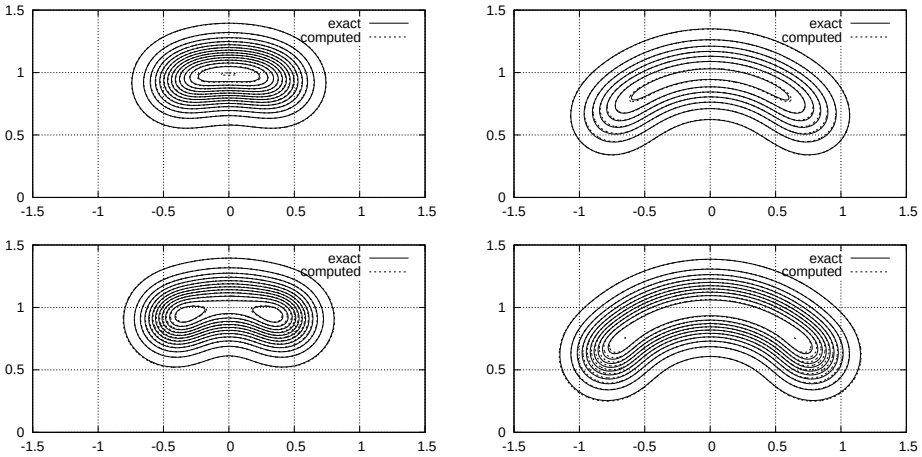

Figure 5: Mean (top row) and standard deviation (bottom row) of the scalar field after 1 revolution (left) and 2 revolutions (right). Plotted are the particle solution (No $= 20$) and the exact solution. Contour levels start at $\Delta/2$ with fixed increments Δ, where $\Delta = 0.2$.

We now focus on the conservation of first invariants in the numerical solution. Since the initial condition is deterministic, we have for for all time

$$I(0) = \sum_{i=1}^{\mathrm{Np}} [C_i]_0 = 1, \quad I(k) = \sum_{i=1}^{\mathrm{Np}} [C_i]_k = 0, \ k \geq 1. \tag{67}$$

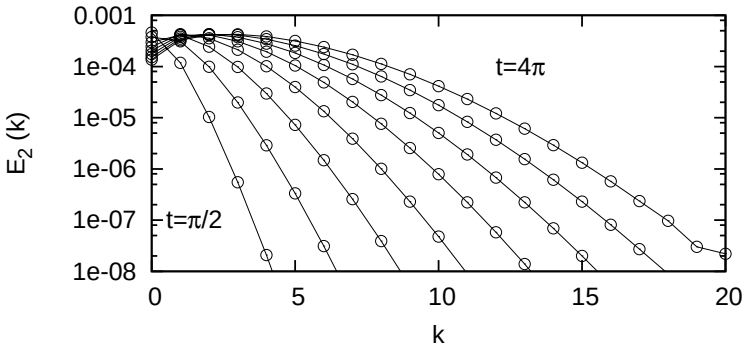

Figure 6: Spectrum $E_2(k)$, as defined in (66), of the particle solution for No = 20. Curves are generated at every quarter revolution.

The proposed method being conservative at the discrete level, it is expected that these invariants are also conserved in the computations. However, due to remeshing, this is not necessarily the case. Specifically, in order to avoid an unreasonable increase in the number of particles, only particles with strengths exceeding a predetermined threshold are retained after remeshing, while others are discarded. As a result, the invariants are not exactly conserved. The error that is incurred depends on the threshold value used to decide whether particles are kept or omitted. In the present computation, this criterion consists of discarding particles whose strength satisfy $|[C_i]_k| < 10^{-8}$ for all k. Figure 7 shows the evolution $|I(k)|$ as a function of the number of revolutions for even modes, $k \geq 2$. It is observed that the invariants $I(k > 0)$ do in fact vary with time. Similar observation is made for the odd modes, which however have smaller magnitudes. However, the conservation "errors" associated with the first invariants are small, particularly compared to the energies $E_2(k)$, and consequently deemed acceptable. Thus, further refinement of the remeshing procedure was not attempted. Note that due to the uncertainty in the convective field, the domain covered by the particles must extend beyond the support of a single realization (or in other words the support of the initial distribution). This is achieved during remeshing, specifically through the introduction of additional particles around the boundaries of the prevailing particle distribution. As is the case for particle removal, the introduction of new particles depend on the selected tolerance. Numerical tests have shown that conservation of the invariants considered above improves by lowering the tolerance level. However, this improvement comes at the cost of a significant increase in the number of particles and with only small improvement of the statistics, as more resources are added in regions where the scalar modes are very small. This is illustrated in Figure 7, which simultaneously depicts the particle distribution and contours of the variance in the scalar field. In particular, the figure indicates that the region where significant variance occurs is contained well within the region covered by the particles, and thus the addition of new particles is beyond the point of di-

minishing returns. These observations also justify the selection of the tolerance value.

In another series of numerical tests, the order of the PC expansion was progressively decreased while keeping constant the parameters of the particle discretization. The aim was to assess the robustness of the predictions to under-resolved polynomial expansions. Spectra for No = 10 and No = 5 are plotted in Figure 8, and are contrasted with previous predictions obtained with No = 20. The comparison shows that with No = 10 the predictions can be considered to be suitably resolved up to 1.5 revolutions, while for No = 5 the resolution becomes insufficient after just 3/4 of revolution. Truncation to lower order essentially affects the highest mode, while for $k <$ No the energy is nearly unaffected by the selected value of No. Additional insight into the impact of expansion order can be gained from Figure 9, which depicts contours at $t = 4\pi$ of mode $k = 4$ computed using No = 5 and 10, and of mode $k = 9$ computed with No = 10 and No = 20. It is seen that with No = 5 the prediction of mode 4 is clearly corrupted. For mode 9, the predictions obtained with No = 10 and 20 are close, though noticeable differences are still observed. The impact of resolution effects can also be appreciated from Figure 10, which illustrates the standard deviation fields for different orders at the end of the computations.

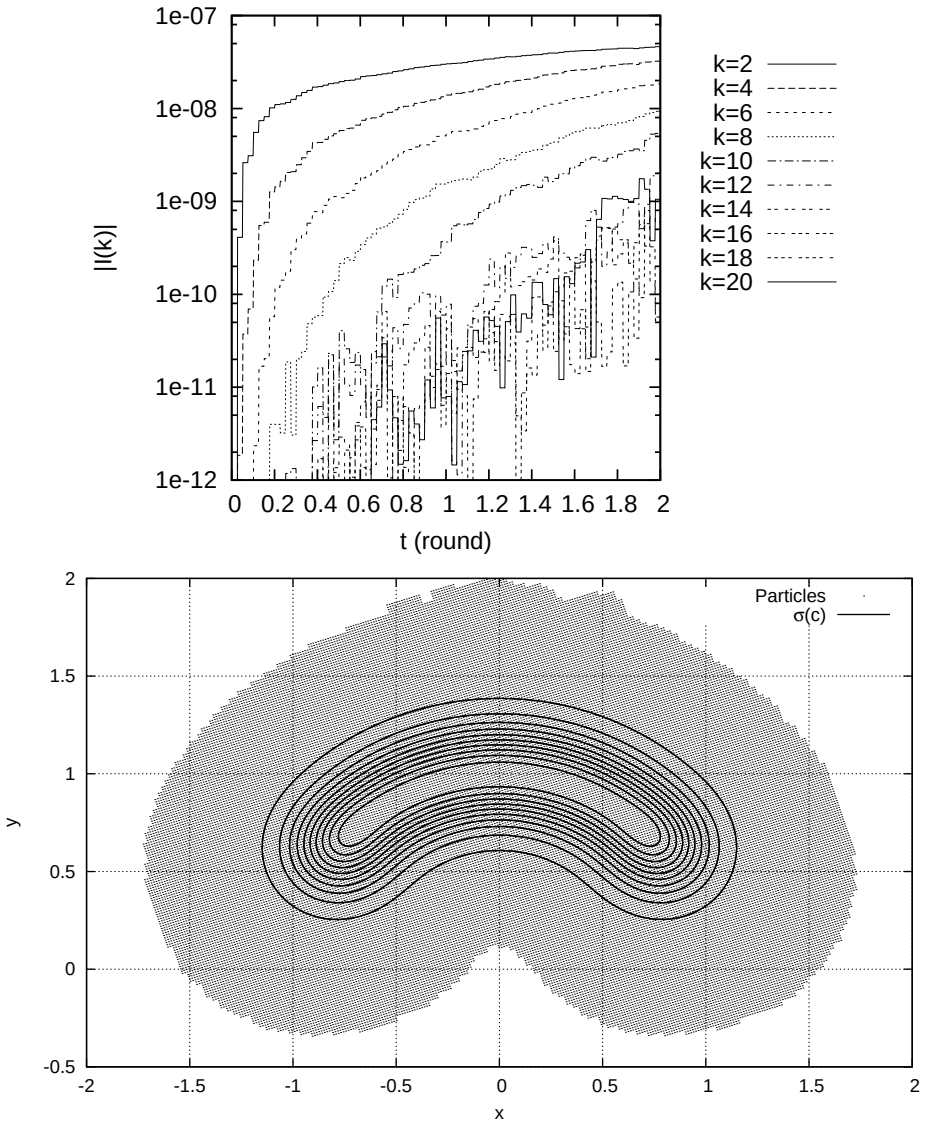

Figure 7: Top: evolution of the first invariants of the even modes $I(k)$. Bottom: distribution of the particles after 2 revolutions. Also plotted are the iso-lines of the standard deviation of c at the same time; contours levels start at 0.15 with constant increment 0.3. The number of particles Np $\sim 39,500$, whereas only 15,000 particles were present at the start of the computations.

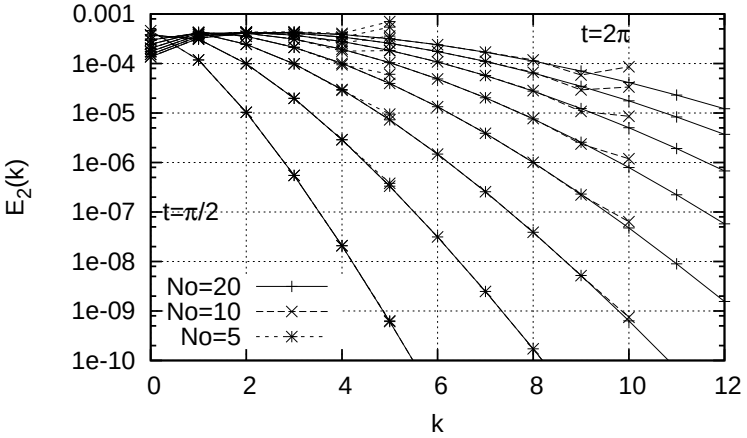

Figure 8: Comparison of the spectra $E_2(k)$ at different times and computed for stochastic expansions truncated at different order No = 20, 10 and 5.

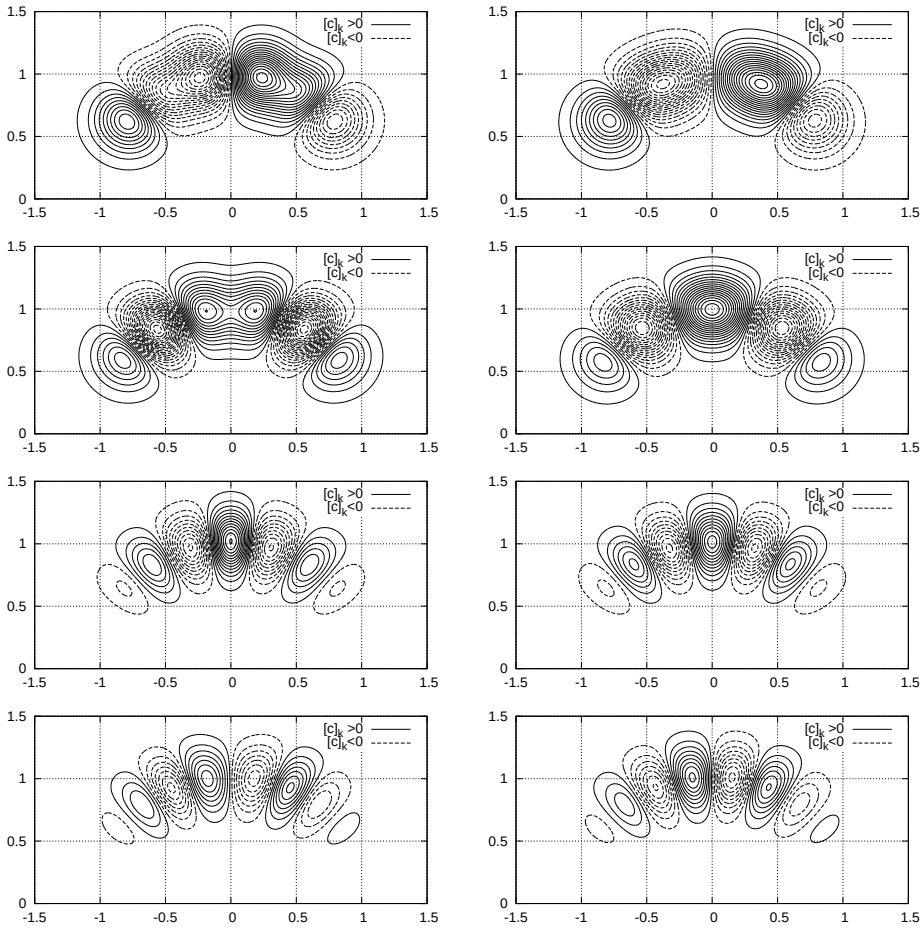

Figure 9: Top row: isolines of $[c]_4$, computed with expansion orders No = 5 (left) and No = 10 (right). Second row: isolines of $[c]_5$, computed with expansion orders No = 5 (left) and No = 10 (right). Third row: isolines of $[c]_9$, computed with expansion orders No = 10 (left) and No = 20 (right). Fourth row: isolines of $[c]_{10}$, computed with expansion orders No = 10 (left) and No = 20 (right). In all cases, the computed solutions at $t = 4\pi$ are used; isolines start at ± 0.1 with constant increment ± 0.2.

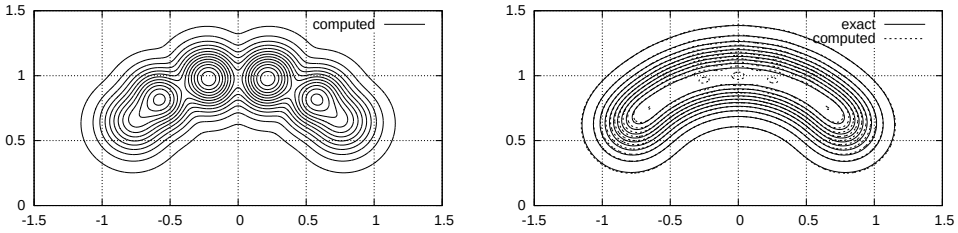

Figure 10: Isolines of standard deviation in c at $t = 4\pi$, computed with expansions truncated at No = 5 (left) and No = 10 (right). Also plotted on the right is the standard deviation of the exact solution. Isolines start at 0.1 with constant increment 0.2

5 Application to natural convection

In this section, we discuss the implementation of the stochastic mesh-particle scheme to simulate the evolution of a localized hot patch of fluid in an infinite domain. The initial conditions are:

$$\omega(\boldsymbol{x}, t=0) = 0, \quad \theta(\boldsymbol{x}, t=0) = \exp\left(-10r^8\right), \quad r = |\boldsymbol{x}|. \tag{68}$$

For the range of Rayleigh numbers considered here, the evolution of the flow that can be summarized as follows. At early stages, the hot patch starts to rise due to buoyancy, and a pair of counter-rotating vortices is created on its sides. The flow induced by the vortices distorts the patch, and the latter experiences higher velocities at its centerline. As time increases, the distortion becomes more pronounced and the patch is strained in a filament trapped in the two rolling vortices. At the centerline, a smaller secondary patch of hot fluid subsequently detaches, and a second pair of counter-rotating vortices is formed; see Figures 12 and 13 below.

One can easily draw a qualitative picture of the dependence with the Rayleigh number of these processes summarized above. For instance, at lower Rayleigh numbers one would expect less energetic vortices, as higher mixing rates would occur during the rollup process. The eventual interruption of successive detachments and rollups due to viscous stabilization would also be anticipated. However, from a quantitative perspective, prediction of the dependence of even integral quantities on variabilty in the Rayleigh number is more challenging. Indeed, variability in the Rayleigh number not only affects diffusion rates (as in section4.1), the convective field (as in section 4.2), but also the complex coupling between the thermal and convective fields.

To investigate these effects, the full set of Boussinesq equations is solved. The Prandtl number Pr = 0.71. An uncertain Rayleigh number is considered, $\mathrm{Ra} = 2.5\ 10^5 \pm 5.10^4$, and once again a uniform pdf is assumed, leading to the following one-dimensional Legendre expansion:

$$\mathrm{Ra}(\xi) = [\mathrm{Ra}]_0 + [\mathrm{Ra}]_1 \xi = 2.5\ 10^5 + 5.10^4 \xi, \quad p(\xi) = \begin{cases} 1/2, \ \xi \in [-1,1] \\ 0, \ \text{otherwise} \end{cases}.$$

Evaluation of the PC expansion of the factor $1/\sqrt{\mathrm{Ra}}$, which features in the governing equations, is performed in two steps. First, the expansion of $1/\mathrm{Ra}$ is computed by inverting the exact Galerkin product [25, 11]:

$$\mathrm{Ra} \times \frac{1}{\mathrm{Ra}} = \sum_k \left(\sum_l \sum_m C_{klm} [\mathrm{Ra}]_l \left[\frac{1}{\mathrm{Ra}}\right]_m \right) \Psi_k \equiv 1\Psi_0. \tag{69}$$

Second, the expansion of the square root of $1/\mathrm{Ra}$ is extracted by solving a non-linear system of equations expressing again the Galerkin product [11]:

$$\sum_l \sum_m C_{klm} \left[\frac{1}{\sqrt{\mathrm{Ra}}}\right]_l \left[\frac{1}{\sqrt{\mathrm{Ra}}}\right]_m = \left[\frac{1}{\mathrm{Ra}}\right]_k, \quad k = 0, \ldots, \mathrm{No}. \tag{70}$$

To extract the "positive" square root, an iterative Newton method is employed with starting values $\left[1/\sqrt{\mathrm{Ra}}\right]_0 = 1/\sqrt{[\mathrm{Ra}]_0}$ and $\left[1/\sqrt{\mathrm{Ra}}\right]_{k>0} = 0$. The resulting probability density function of $1/\sqrt{\mathrm{Ra}}$ is plotted in Figure 11; a PC expansion with No = 12 is used. The PC approximation of $1/\sqrt{\mathrm{Ra}}$ is also reported in Figure 11, which indicates that the flow will be less diffusive as ξ increases. Also note that $\left\langle 1/\sqrt{\mathrm{Ra}} \right\rangle \sim 2.01\ 10^{-3}$ slightly differs from $1/\sqrt{\langle \mathrm{Ra} \rangle} = 2\ 10^{-3}$.

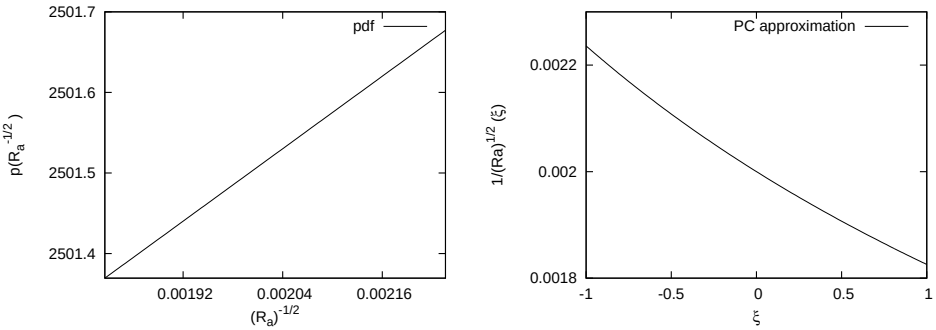

Figure 11: Left: probability density function of $1/\sqrt{\mathrm{Ra}}$. Right: PC approximation of $1/\sqrt{\mathrm{Ra}}(\xi)$.

In the computations, we set $\epsilon = 1/30$, and remesh spacing $\sqrt{S} = \epsilon/2$. The mesh has spacing $h_g = \epsilon$, giving an average of 4 particles per cell. Time integration is performed by applying the second-order Adams-Bashforth scheme, with time step $\Delta t = 0.2$, except for iterations that immediately follow remeshing, where a second-order Runge-Kutta scheme is employed. Remeshing is performed every 4 iterations.

Figure 12 compares the mean temperature field $[\theta]_0$ with the deterministic temperature field corresponding to the mean Rayleigh number $\langle \mathrm{Ra} \rangle$, at times $t = 10$ and $t = 20$. At the early time $t = 10$, the two fields are nearly identical, the stochastic mean field just being slightly smoother than the deterministic prediction. On the contrary, at $t = 20$ noticeable differences appear, particularly in the zone of high shear around the primary vortex, in the core of the secondary vortices, and at the centerline of the leading hot spot. As discussed previously, these differences arise due to the non-linearity of the flow, as well as the small differences in the mean diffusion coefficient and the square root of the inverse mean Rayleigh number. Similar conclusions can be drawn from the inspection of the corresponding mean and deterministic vorticity fields compared in Figure 13. Note how the size and location of the mean secondary vortices are affected by the variability in Ra.

Additional insight into the variability of the flow is sought through the analysis of the standard deviations of the fields. Figure 14 shows the mean and standard deviation of the temperature field, and the magnitude and standard deviation of the vorticity field at $t = 20$. Only half of the domain is shown, as

the temperature field is symmetric with respect to the axis $x = 0$, whereas the vorticity field is antisymmetic. For the temperature field, it is observed that the areas of greatest variability are located on the centerline of the leading patch of hot fluid and on the external sides of the fluid entrained by the primary vortex. Note that in some areas the temperature standard deviation is as high as one third of the local mean. In other areas, however, such as the core of the primary vortex, only small variability of the temperature occurs. Similar trends can be observed for the vorticity field, though higher variation is noted around the edges of the primary vortex where vorticity filaments of opposite sign are rolling up. In these regions, variability in Ra has a significant influence on the vortex roll-up, and the location of the filament structures has a high level of uncertainty.

To assess the performance of the particle-mesh scheme, we plot in Figure 15 the evolution of Np as well as the particle distribution at $t = 20$. The number of particles increases steadily with time, which is expected since the support of the stochastic solution is also increasing. At $t = 20$, the number of particles $\mathrm{Np} \sim 150,00$ whereas $\mathrm{Np} = 13,000$ at the start of the computations. Also note that the particle distribution properly covers the support of the mean and standard deviation fields depicted earlier, and even extends into regions where the solution modes are essentially vanishing. Thus, a less conservative criterion for particle removal could have safely been used. Also note that the computation simulation was actually carried up to $t = 27.5$, time at which the number of particles exceeded than $200,000$. The CPU time used on a desktop PC was about 10 hours. Thus, the present experience shows that the overhead due to stochastic polynomial expansion can be manageable, even when a large number of particles is used.

As mentioned previously, a PC expansion with $\mathrm{No} = 12$ was used in the present simulation. In order to verify the suitability of the expansion, we plot in Figure 16 the spectra of the vorticity and temperature fields. From these spectra, it can be concluded that the expansion is clearly over-resolved at early times ($t \leq 7$), where a third- or fourth-order expansion would have been sufficient. The energy of the low-order stochastic modes slowly increases up to $t \sim 7$, when a first transition occurs, after which the energy increases at a higher pace. This time actually corresponds to the formation of the primary vortices. The primary vortices then experience a lower rise velocity than the bulk of the hot fluid, and filamentation around its core occurs (see Figure 13). This is accompanied by the sharp increase of the mode energies during the period $t \in [8, 13]$. At later stages, after detachment of the primary vortices, the energy of the stochastic modes levels off. Around $t = 17 \sim 18$, the formation of the secondary vortices begins, and the higher order modes $k > 8$ again experience a rapid growth up to the time at which the secondary vortices detach. Note that during this process the lower order modes are less affected than the higher order modes. Consequently, the stochastic dynamics lead to flatter and broader spectra as time advances, denoting the need for additional modes for suitable resolution. For instance, between $t = 10$ and $t = 20$ the energy ratio between modes 1 and 12 has reduced from more than 10 order of magnitude

to about 6. Overall, the expansion order was deemed sufficient, and this was verified through inspection of the spatial structure of the stochastic modes (not shown), and their rapid decay with increasing mode number.

As a final check of the simulation accuracy, the errors on the first invariant of the temperature modes $I_\theta(k)$ are plotted in Figure 17. The evolution of the invariant errors is reported only for the temperature modes, as the vorticity modes are anti-symmetric and thus the first-order errors tend to naturally balance out. Figure 17 shows that the errors increase steadily, with small modulation during vortex formation. As discussed in the previous section, these errors are entirely due to the remeshing scheme, which in particular removes particles with low strengths. However, it is seen that the error on the invariants are low and are smaller than 10^{-7} for all modes. Compared to the mean thermal energy of the system, $I_\theta(k=0) = 1.6$, the first order errors are evidently negligible.

In the analysis above, we have focused on the first and second statistical moments of the solution. One should note, however, that the PC expansion provides the local probability law of any observable (functional) of the flow variables. In particular, since in the present problem the input uncertainty is bounded, the stochastic representation readily yields estimates of temperature maxima at any point of the domain. As an example, we show in Figure 18 the local sensitivities S_θ and S_ω of the temperature and vorticity fields at $t = 20$. The sensitivity of θ is defined by:

$$S_\theta = \left.\frac{\partial\theta}{\partial \mathrm{Ra}}\right|_{\mathrm{Ra}=\langle\mathrm{Ra}\rangle} = \frac{\partial\theta}{\partial\xi}\left(\frac{\partial \mathrm{Ra}}{\partial\xi}\right)^{-1}\Bigg|_{\xi=0} = \frac{1}{[\mathrm{Ra}]_1}\left.\frac{\partial\theta}{\partial\xi}\right|_{\xi=0}.$$

Using the PC expansion of θ and the particle approximation, the local sensitivity at point $\boldsymbol{x}$ around $\langle\mathrm{Ra}\rangle$ is

$$S_\theta(\boldsymbol{x}) = \sum_{k=0}^{\mathrm{No}}\sum_{i=1}^{\mathrm{Np}} \eta_\epsilon(\boldsymbol{x}-\boldsymbol{X}_i)[\Theta_i]_k \frac{\partial\Psi_k}{\partial\xi}(\xi=0).$$

Note that this sensitivities could be estimated at any Ra value in the uncertainty range.

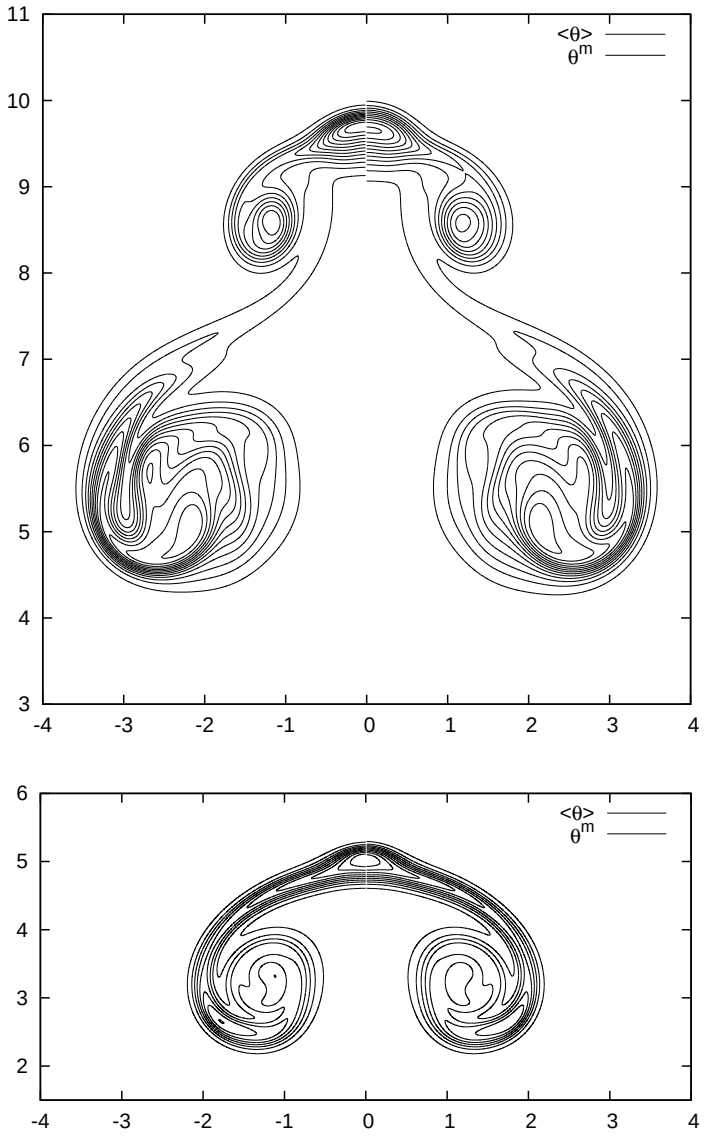

Figure 12: Contours of the mean temperature field $\langle\theta\rangle$, for $x > 0$ (right half), and of the deterministic temperature field θ^m, for $x < 0$ (left half) corresponding to the mean Rayleigh number $\langle \mathrm{Ra} \rangle$. Top: solutions at $t = 20$ with levels starting at 0.01 with constant increment 0.02. Bottom: solutions at $t = 10$, with levels starting at 0.03 with constant increment 0.06.

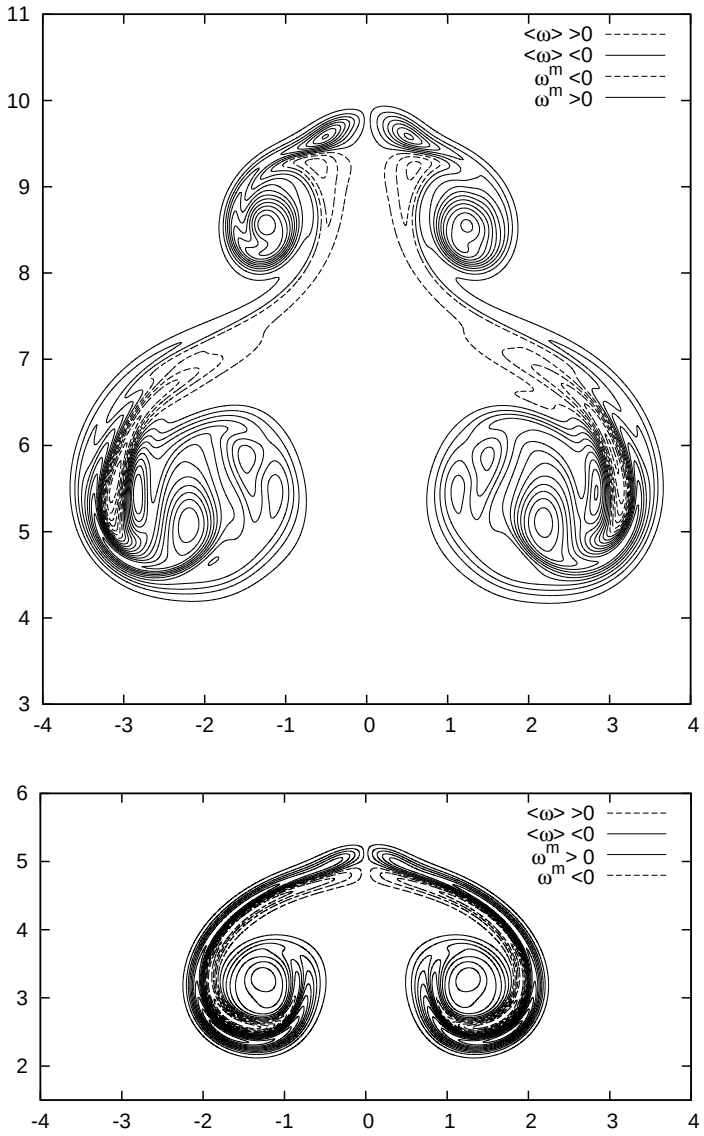

Figure 13: Contours of the mean stochastic vorticity field $\langle\omega\rangle$, for $x > 0$ (right half), with the deterministic vorticity field ω^m, for $x < 0$ (left half), corresponding to the simulation using $\langle \mathrm{Ra} \rangle$. Top: solutions at $t = 20$ with levels starting at ± 0.1 with constant increment ± 0.2. Bottom: solutions at $t = 10$ with levels starting at 0.25 with constant increment 0.5.

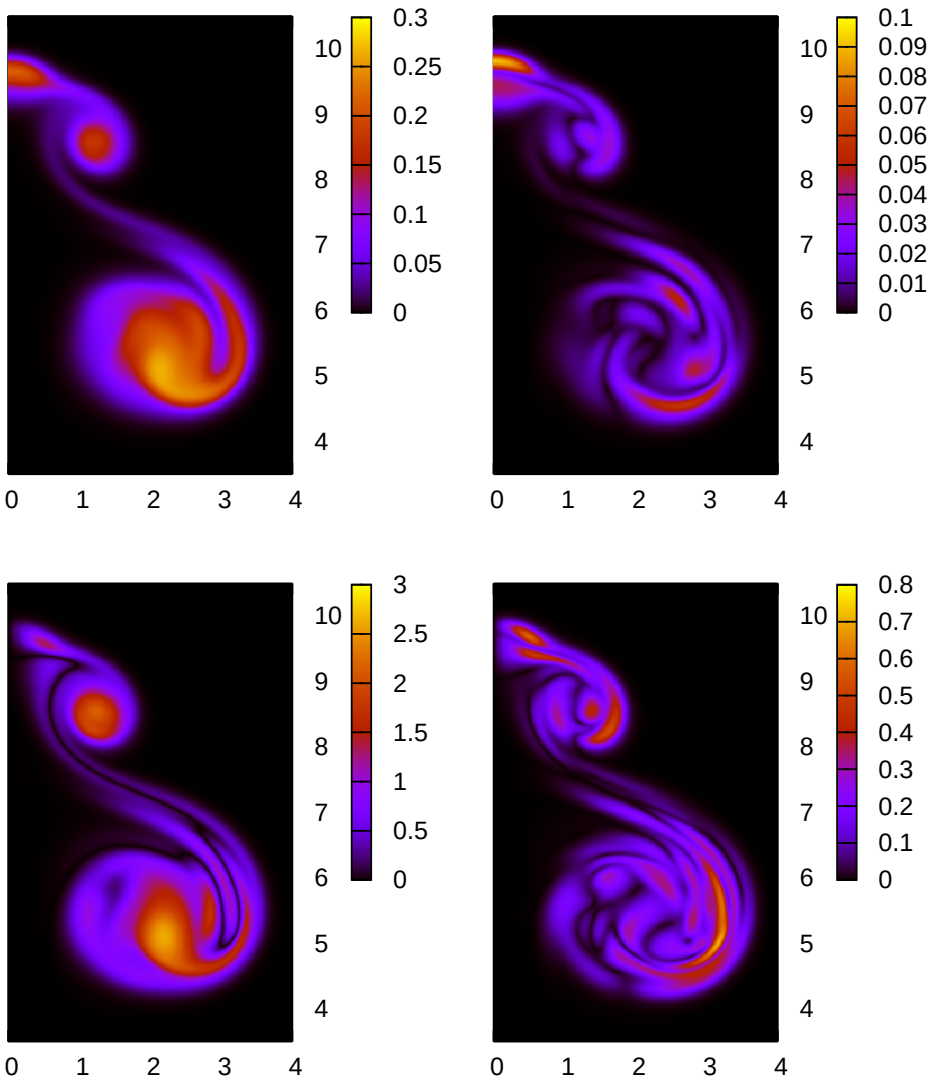

Figure 14: Top: mean temperature field $[\theta]_0$ (left) and standard deviation (right) at $t = 20$ (left). Bottom: magnitude of the mean vorticity field $|[\omega]_0|$ (left) and standard deviation of ω (right) at $t = 20$.

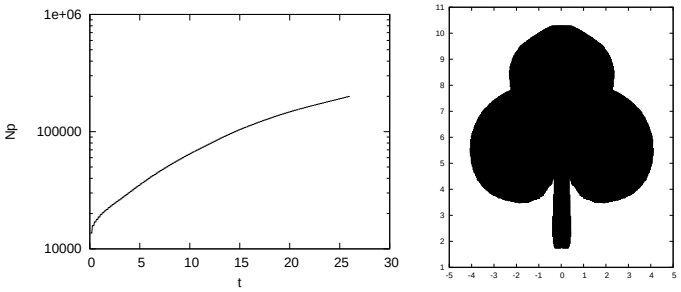

Figure 15: Evolution of the number of particles in the simulation, and the particle distribution at $t = 20$.

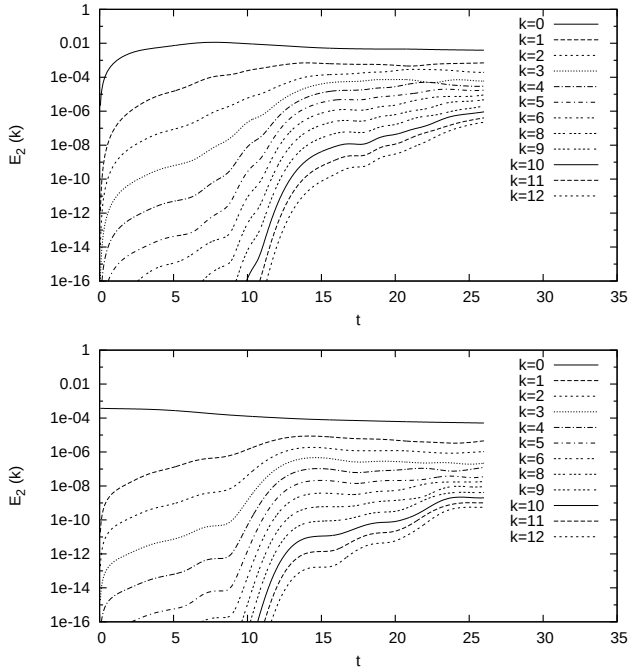

Figure 16: Evolution of energies of the stochastic modes of vorticity (top) and temperature (bottom).

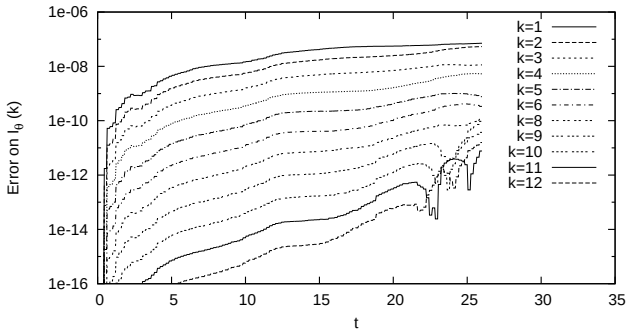

Figure 17: Evolution with time of the absolute error in the first invariant of the temperature modes.

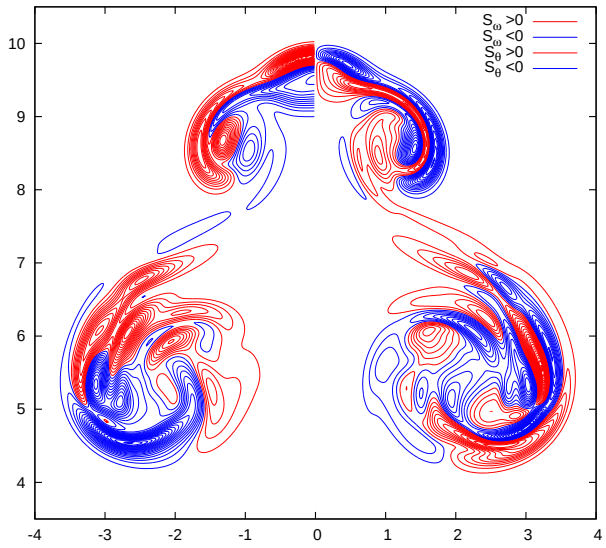

Figure 18: Iso-contours of local sensitivity in temperature (left half of the plot, $x < 0$) and vorticity (right half, $x > 0$) with regard to Ra about $\langle \mathrm{Ra} \rangle$. Contours starts at $\pm\Delta$ with successive increments Δ. $\Delta = 1.5 \times 10^{-7}$ for temperature and $2 \times 10^{-}6$ for vorticity.

6 Conclusion

A new method for parametric uncertainty quantification in fluid flow has been proposed in the context of Lagrangian particle methods. The method combines the advantages and flexibility of particle discretizations (mesh-less, robustness, stability, low diffusivity, ...) with efficient uncertainty representations involving PC expansions.

The essential feature of the method is the use of a single set of particles to transport the stochastic modes of the solution. The Lagrangian positions of the particles are updated using the mean velocity field. This approach overcomes the difficulties that would arise if different sets of particles are defined for different modes. It further allows for the re-use of fast methods, including particle-mesh techniques. Another key aspect of the method is the conservative character at the discrete level of the treatment of the interaction between stochastic modes. The discretization was found to be stable and essentially diffusion-free, thus allowing uncertainty quantification in slightly viscous flow, and transport at high, or even infinite Péclet numbers by uncertain velocity fields. These properties were shown on the basis of idealized validation problems and illustrated by a larger scale computation showing that the method can deal efficiently and accurately with complex flows involving a large number of particles.

The present work has focused on a basic construction that combines a particle-mesh scheme with uncertainty quantification method based on the PC formalism, and applications of the resulting stochastic scheme were restricted to unbounded flows. Additional work is consequently needed to extend the formulation to more general conditions and gain better understanding of the the range of possible applications. For instance, generalization of the formulation to accommodate solid boundaries would be desirable. This could be achieved, for instance, by adapting the scheme of Koumoutsakos et al. [19], in which a linear problem for the vorticity flux across the boundary is solved at each time-step. Application of the PC formalism to this scheme would result in a set of decoupled problems for the stochastic vorticity modes, thus preserving the features of the deterministic formulation. Another possible refinement of the present construction concerns the remeshing algorithm. In particular, more elaborate constructions should be sought, which would improve accuracy and allow conservation of flow invariants. In particular, accurate approaches developed for deterministic flows [8] appear to be readily amenable to PC expansions using the presently developed framework.

A Projection and interpolation schemes

In the projection step, the value of the vorticity field at the mesh points is computed based on knowledge of the particle positions and strengths. The mesh is a uniform grid with cell size h_g in each direction. The vorticity value at a grid point $\boldsymbol{x}_g = (x_g, y_g)$ is expressed as:

$$\omega(\boldsymbol{x}_g) = \sum_{i=1}^{M} \frac{\Gamma_i}{h_g^2} \Lambda\left(|x_g - X_i|/h_g\right) \Lambda\left(|y_g - Y_i|/h_g\right),$$

where

$$\Lambda(u) = \begin{cases} (1-u^2)(2-u)/2, & \text{if } 0 \le u < 1; \\ (1-u)(2-u)(3-u)/6, & \text{if } 1 \le u \le 2; \\ 0 & \text{otherwise.} \end{cases}$$

The strength of a particle is therefore distributed on the 16 nearest mesh points.

To interpolate the mesh velocity onto the particles, the same interpolation scheme is used. Specifically, we have:

$$\boldsymbol{u}(\boldsymbol{X}_i) = \sum_{g} \boldsymbol{u}(\boldsymbol{x}_g) \Lambda\left(|x_g - X_i|/h_g\right) \Lambda\left(|y_g - Y_i|/h_g\right),$$

where the summation index g runs over all the mesh points index.

References

[1] J.T. Beale. On the accuracy of vortex methods at large times. In *Computational Fluid Dynamics and Reacting Gas Flows*. Springer-Verlag, 1988.

[2] A. Beaudouin, S. Huberson, and E. Rivoalen. Simulation of anisotropic diffusion by means of a diffusion velocity method. *J. Comput. Physics*, 186:122–135, 2003.

[3] R.H. Cameron and W.T. Martin. The orthogonal development of nonlinear functionals in series of Fourier-Hermite functionals. *Ann. Math.*, 48:385–392, 1947.

[4] J.P. Choquin and B. Lucquin-Desreux. Accuracy of a deterministic particle method for Navier-Stokes equations. *J. Num. Meth. Fluids*, 8:1439–1458, 1988.

[5] A. Chorin. Numerical study of slightly viscous flow. *J. Fluid Mech.*, 57:785–796, 1973.

[6] I.P. Christiansen. Numerical simulation of hydrodynamics by the method of point vortex. *J. Comput. Physics*, 13(3):363–379, 1973.

[7] G.H. Cottet. Large time behavior of deterministic particle approximations to the Navier-Stokes equations. *Math. Comp.*, 56:45–59, 1991.

[8] G.H. Cottet and P. Koumoutsakos. *Vortex Methods Theory and Practice*. Cambridge University Press, 2000.

[9] G.H. Cottet and S. Mas-Gallic. A particle method to solve the Navier-Stokes system. *Numer. Math.*, 57:805–827, 1990.

[10] B. Debusschere, H.N. Najm, A. Matta, O.M. Knio, R.G. Ghanem, and O.P. Le Maître. Protein labeling reactions in electrochemical microchannel flow: Numerical prediction and uncertainty propagation. *Physics of Fluids*, 15(8):2238–2250, 2003.

[11] B.J. Debusschere, H.N. Najm, P.P. Pébray, O.M. Knio, R.G. Ghanem, and O.P. Le Maître. Numerical challenges in the use of Polynomial Chaos representations for stochasic processes. *SIAM Journal on Scientific Computing*, 26(2):698–719, 2004.

[12] P. Degond and S. Mas-Gallic. The weighted particle method for convection diffusion equations - part 1 : The case of an isotropic viscosity. *Math. Comput.*, 33(53):485–507, 1989.

[13] P. Degond and F. J. Mustieles. A deterministic approximation of diffusion using particles. *SIAM Journal on Scientific Computing*, 1(2):293–310, 1990.

[14] J.D. Eldredge, A. Leonard, and Colonius T. A general deterministic treatment of derivatives in particles methods. *J. Comput. Physics*, 180:686–709, 2002.

[15] R. Ghanem and S. Dham. Stochastic finite element analysis for multiphase flow in heterogeneous porous media. *Transp. Porous Media*, 32:239–262, 1998.

[16] R.G. Ghanem and P.D. Spanos. *Stochastic Finite Elements: A Spectral Approach*. Dover, 2002. 2nd edition.

[17] T.D. Hien and M. Kleiber. Stochastic finite element modeling in linear transcient heat transfer. *Comp. Met. App. Mech. Eng.*, 144:111–124, 1997.

[18] O.M. Knio and O.P. Le Maître. Uncertainty propagation in CFD using polynomial chaos decomposition. *Fluid Dyn. Res.*, 38:616–640, 2006.

[19] P. Koumoutsakos, A. Leonard, and P. Pépin. Boundary conditions for viscous vortex methods. *J. Comput. Physics*, 113:52–61, 1994.

[20] A. Leonard. Vortex methods for flow simulations. *J. Comput. Physics*, 37:289–335, 1980.

[21] O.P. Le Maître. Polynomial chaos expansion of a lagrangian model for the flow around an airfoil. *C. R. Mecanique*, 2006. in press.

[22] O.P. Le Maître, O.M. Knio, H.N. Najm, and R.G. Ghanem. A stochastic projection method for fluid flow. i. basic formulation. *J. Comput. Phyics*, 173:481–511, 2001.

[23] O.P. Le Maître, O.M. Knio, H.N. Najm, and R.G. Ghanem. Uncertainty propagation using Wiener-Haar expansions. *J. Comput. Phyics*, 197(1):28–57, 2004.

[24] O.P. Le Maître, H.N. Najm, R.G. Ghanem, and O.M. Knio. Multi-resolution analysis of Wiener-type uncertainty propagation schemes. *J. Comput. Physics*, 197(2):502–531, 2004.

[25] O.P. Le Maître, M.T. Reagan, B. Debusschere, H.N. Najm, R.G. Ghanem, and O.M. Knio. Natural convection in a closed cavity under stochastic, non-Boussinesq conditions. *SIAM Journal on Scientific Computing*, 26(2):375–394, 2004.

[26] O.P. Le Maître, M.T. Reagan, H.N. Najm, R.G. Ghanem, and O.M. Knio. A stochastic projection method for fluid flow. ii. random process. *J. Comput. Phyics*, 181:9–44, 2002.

[27] P.A. Raviart. An analysis of particles methods. *Lecture Notes in Math.*, 1127:243–324, 1985.

[28] M.T. Reagan, H.N. Najm, R.G. Ghanem, and O.M. Knio. Uncertainty quantification in reacting flow simulations through non-intrusive spectral projection. *Combustion and Flames*, 132:545–555, 2003.

[29] E. Rivoalen and S. Huberson. Numerical simulation of axisymmetric flows by means of a particle method. *J. Comput. Physics*, 152:1–31, 1999.

[30] L. Rosenhead. The formation of vortices from a surface of discountinuity. *Proc. Royal Society*, 134, 1931.

[31] X. Wan and G.E. Karniadakis. An adaptative multi-element generalized polynomial chaos method for stochastic differential equations. *J. Comput. Physics*, 209:617–642, 2005.

[32] S. Wiener. The Homogeneous Chaos. *Amer. J. Math.*, 60:897–936, 1938.

[33] D.B. Xiu and G.E. Karniadakis. The Wiener-Askey Polynomial Chaos for stochastic differential equations. *SIAM Journal on Scientific Computing*, 24:619–644, 2002.

[34] D.B. Xiu and G.E. Karniadakis. Modeling uncertainty in flow simulations via generalized Polynomial Chaos. *J. Comput. Physics*, 187:137–167, 2003.